BJR

Received:
14 August 2014

Revised:
4 November 2014

Accepted:
18 November 2014

doi: 10.1259/bjr.20140547

Cite this article as:
Zhu B, Sevick-Muraca EM. A review of performance of near-infrared fluorescence imaging devices used in clinical studies. Br J Radiol 2015;88: 20140547.

REVIEW ARTICLE

A review of performance of near-infrared fluorescence imaging devices used in clinical studies

B ZHU, PhD and E M SEVICK-MURACA, PhD

Center for Molecular Imaging, The Brown Foundation Institute of Molecular Medicine, The University of Texas Health Science Center, Houston, TX, USA

Address correspondence to: Professor Eva M Sevick-Muraca
E-mail: *Eva.Sevick@uth.tmc.edu*

ABSTRACT

Near-infrared fluorescence (NIRF) molecular imaging holds great promise as a new "point-of-care" medical imaging modality that can potentially provide the sensitivity of nuclear medicine techniques, but without the radioactivity that can otherwise place limitations of usage. Recently, NIRF imaging devices of a variety of designs have emerged in the market and in investigational clinical studies using indocyanine green (ICG) as a non-targeting NIRF contrast agent to demark the blood and lymphatic vasculatures both non-invasively and intraoperatively. Approved in the USA since 1956 for intravenous administration, ICG has been more recently used off label in intradermal or subcutaneous administrations for fluorescence imaging of the lymphatic vasculature and lymph nodes. Herein, we summarize the devices of a variety of designs, summarize their performance in lymphatic imaging in a tabular format and comment on necessary efforts to develop standards for device performance to compare and use these emerging devices in future, NIRF molecular imaging studies.

Near-infrared fluorescence (NIRF) imaging is an emerging clinical technology that requires administration of a fluorescence-imaging agent that can be excited at near-infrared (NIR) wavelengths of $\geq$760 nm. Upon illuminating tissue surfaces with penetrating NIR light to excite the imaging agent within the tissues, the generated fluorescence is collected to form a two-dimensional (2D) image demarking the tissue deposition of the NIRF imaging agent. While far-red and NIR light between the wavelength ranges of 690–900 nm penetrate deeply in tissues, endogenous chromophore fluorescence when excited by light of wavelengths $<$780 nm, creates a high autofluorescence background for molecularly targeting exogenous imaging agents in tissues. The tissue depth to which the NIRF imaging can detect NIRF imaging agents is dependent upon their brightness and the sensitivity of the device, but has been estimated to be between 3 and 4 cm beneath the tissue surfaces in intensified devices[1] and $<$2 cm in others.[2] Three-dimensional tomographic imaging using 2D projection data as well as time-dependent and independent methods has been developed for small animal imaging[3,4] but, owing to these limitations in tissue penetration, has not been translated to clinical imaging.

The exciting concept of conjugating a NIR excitable fluorophore to a small molecule, protein or antibody that targets an extracellular disease marker for diagnostic, molecular imaging has been postulated for years by several investigators.[5–7] The use of NIRF imaging for molecularly guided surgical resection of cancers could dramatically reduce residual tumour burden as well as surgical morbidity associated with excising sufficient tissues to avoid having positive surgical margins. However, the tissue depth, concentration and dose at which a "first-in-humans" imaging agent can be detected in tissues depends upon several factors but, most importantly, upon the sensitivity of the imaging device. Unlike positron emission tomography, scintigraphy, single-photon emission and the γ probe used to detect radiolabelled molecular targeting agents for diagnostic imaging and intraoperative detection, fluorescence imaging devices do not have phantoms and standards to assess performance metrics, and there are no traceable standards to quantify or compare performance between fluorescence imaging devices. Different fluorescent imaging device designs, summarized for clinical devices in an excellent review by Alander et al,[8] likely result in varying performance for detecting a NIRF imaging agent. As a result in the USA, the regulatory strategy for securing market approval of

fluorescent imaging agents is to pair the drug approval process to a specific model of imaging device [*e.g.* approval of Cysview® (Photocure, Oslo, Norway) with Karl Storz blue light cystoscope (PDD system; Karl Storz GmbH and Co., Tuttlingen, Germany)]. This practice could limit the entry and adoption of molecularly targeted NIRF imaging agents into clinical practice.

To date, the only NIR-excited fluorophore used clinically is indocyanine green (ICG). Since 1956, ICG has been approved by the US Food and Drug Administration for intravenous (i.v.) administration at a concentration of 2.5 mg ml^{-1} with doses of up to 25 mg in adults, 12.5 mg in children and 6.25 mg in infants. ICG has been used in the clinic as a reagent for determining cardiac output, hepatic function and ophthalmic angiography. It has an excellent record of safety, and there is no demonstrable evidence of phototoxicity associated with its use.[9] After administration, ICG binds tightly to plasma proteins and has a half-life of several minutes in blood circulation, which allows repeated intraoperative i.v. administration for fluorescence angiography. In the plasma, the absorption and emission peaks of ICG are shifted towards longer wavelengths, to around 807 and 822 nm,[10] respectively, but still reside in the "optical window" of the tissues. Compared with other NIR-excited fluorophores, the quantum efficiency (QE) of ICG is low and reported to be 0.02 at 780 nm excitation and 830 nm emission;[11] it is comparatively unstable once reconstituted in saline; and it has no functional group for conjugation to compound for molecular imaging. Using ICG as a non-specific blood vascular imaging agent, NIRF angiography has been used intraoperatively in coronary, neurosurgical and vascular surgeries[8] as well for non-invasive assessment of superficial perfusion.[12]

Most recently, ICG has been used in off-label intradermal and subcutaneous administrations at varying doses for evaluating the lymphatic circulation to identify sentinel lymph nodes (SLNs) in surgical oncology,[10,13,14] assess lymphovenous anastomoses (LVA) surgery[15–17] and non-invasively map the lymphatic vasculature.[18–20] Indeed, "ICG lymphography" has been found to be superior to lymphoscintigraphy for diagnostic imaging of early lymphoedema in upper extremities[20] and enables early diagnosis of lymphoedema before the onset of symptoms.[20–22] Yet, the doses of ICG and the design of devices used in these and other clinical studies vary widely, suggesting variable device performance. The available ICG fluorescence imaging devices on the market include photodynamic eye (PDE; Hamamatsu Photonics Co., Hamamatsu, Japan) and SPY (Novadaq Technologies Inc., Toronto, ON, Canada), with other investigational devices such as frequency-domain photon migration (FDPM) imager (University of Texas Health Science Center at Houston, TX) and mini-FLARE™ (Israel Beth Deaconess Medical Center, Boston, MA) also employed in clinical studies. Although the architecture can be dramatically different among these devices, the core components are (i) the light source for exciting ICG; (ii) optical filters for separating emitted fluorescent signals from strong backscattered excitation light and ambient light signals; and (iii) an area detector for sensing the emitted fluorescent signals. Undoubtedly, the performance of a device is ultimately determined by these core components, requiring different dosages of ICG ranging from micrograms to milligrams per injection for visualizing the lymphatics. In this review, we first compare three core components employed in various ICG fluorescence imaging systems and then review the varying ICG concentrations used in clinical imaging of the lymphatic vasculature and lymph nodes as an indicator of device performance. This review complements those of others[10,13,14,23] but summarizes literature results in a tabulated and quantitative format to enable readers to compare performance. Finally, we comment on a proposal for a systematic approach to quantify and report imaging device performance using standardized measurements of certifiable phantoms that could accelerate the future translation of NIRF molecular imaging agents used with these fluorescence imaging devices.

INSTRUMENTATION

In order to understand differences in performance presented in the ICG imaging of lymph nodes for cancer staging and the Lymphatic imaging sections, the differences in imaging devices employed in these studies are first described. As described in past reviews,[8,24] there are three core components common to the ICG fluorescence imaging systems, summarized in Table 1. These are the incident light sources used to excite ICG; the optics that allow for collection of ICG fluorescence and rejection of ambient and backscattered incident light; and the area detector used to register the collected light (Figure 1).

Incident light sources for collection of indocyanine green fluorescence

The commonly used excitation light sources in ICG fluorescence imaging systems in order of increasing spectral bandwidth are (i) laser diodes; (ii) light-emitting diodes (LEDs); and (iii) filtered lamp sources, which have typical spectra illustrated in Figure 1a. Because rejection of backscattered excitation light is performed spectrally through the use of interference filters, laser diodes enable the greatest sensitivity, since the "background" arising from "leakage" of backscattered excitation light is the lowest. By contrast, LEDs generate a broader band of wavelengths with relatively lower power output, requiring tens of LEDs integrated together for milliwatts per square centimetre of incident light. For the filtered lamp sources, the lamp sources are filtered to generate excitation light with a narrow band, but the generated excessive heat needs to be dissipated to extend the lifetime of the filter. In addition, the filtered lamp sources have low efficiencies, making it difficult to couple into an optical fibre. Hence, laser diodes and LEDs are widely adopted in the ICG fluorescence imaging systems used clinically. One might expect that the greater amount of incident excitation light (measured as a "fluence" in milliwatts per square centimetre) would result in more ICG fluorescence and a larger amount of collected fluorescence signal. However, there are maximum permissible exposure (MPE) limits for both eye safety as well as skin safety. The American National Standards Institute's (#13997) MPE for eye exposure of a 700–1050 nm laser beam is $10^{2(\lambda - 0.700)} \times 10^{-3}$ W cm^{-2} when the duration is between 10 and 30,000 s, and the MPE for skin exposure

Table 1. Summary of various indocyanine green fluorescence imaging devices from excitation source, fluorescence collection, working distance (WD) and field of view (FOV)

Device	Excitation source			Fluorescence collection				WD (cm)	FOV (cm^2)
	Source type	Excitation wavelength λ_e (nm)	Fluence rate ($mW\,cm^{-2}$)	Camera type	Dynamic range (bit)	Integration time (ms)	Collection wavelength λ_c (nm)		
FDPM imager	Laser	785	<1.90	Intensified CCD	16	50–800	825–835	<76.2	<900
Mini-FLARE™	LED	760	7.70	CCD	12	0.1–8000	800–848	10–32	12 × 9 at 32 cm WD
SPY	Laser	806	31 (narrow FOV) 4 (wide FOV)	CCD	8	Real-time video	Centred at 830	30	7.6 × 5.0 19.0 × 12.7
Photodynamic eye	LED	760	4.0	CCD	8	NS	>820	20	10.0 × 6.7
HyperEye Medical System	LED	760–780	NS	CCD	NS	NS	800–850	NS	NS
FLUOBEAM®	Laser	750	5.0	CCD	8	1–1000	>800	15–25	2.2 × 1.5 to 20 × 14
IC-View	Laser	780	Incident power NS	CCD	NS	NS	NS	NS	NS
Visual Navigator	LED	740	Incident power NS	CCD	NS	NS	Centred at 820	NS	NS
The prototype surgical navigation system	LED	760	Incident power NS	Electron-multiplying CCD	16	Real-time video	810–870	60	7.9 × 7.9 to 12.5 × 12.5
Leica FL800	Xenon	700–800	NS	CCD	NS	NS	820–860	NS	NS
INFRARED™ 800™	Xenon	700–780	NS	CCD	NS	NS	820–900	NS	NS
FIREFLY™ for robotic surgery (da Vinci®)	Laser	806	NS	CCD	NS	NS	NS	NS	NS
Laparoscopic near-infrared fluorescence system	Xenon	NS	NS	CCD	NS	NS	NS	NS	NS

CCD, charge-coupled devices; LED, light-emitting diode; NS, not specified.
The devices mentioned in the table and their manufacturer details in parenthesis are as follows: FDPM imager (University of Texas Health Science Center at Houston, TX), FIREFLY for robotic surgery (da Vinci; Novadaq Technologies Inc., Toronto, ON, Canada), FLUOBEAM (Fluoptics, Grenoble, France), HyperEye (Mizuho Medical Co., Ltd, Tokyo, Japan), IC-View (Pulsion Medical Systems SE, Feldkirchen, Germany), INFRARED 800 (Zeiss™; Karl Zeiss Inc., Jena, Germany), Laparoscopic near-infared fluorescence system (Olympus®, Tokyo, Japan), Leica FL800 (Leica Microsystems Inc., Buffalo Grove, IL) Mini-FLARE (Israel Beth Deaconess Medical Center, Boston, MA), Photodynamic eye (PDE; Hamamatsu Photonics Co., Hamamatsu, Japan), SPY (Novadaq Technologies Inc.), The prototype surgical navigation system (Chinese Academy of Sciences, Beijing, China) and Visual Navigator (SH System, Seoul, Republic of Korea).

Figure 1. Schematic of indocyanine green (ICG)-based near-infrared fluorescence imaging system consisting of the incident light source, collection optics and area detector. (a) Represents the spectra of 785-nm laser diode, 780-nm light-emitting diode (LED) and xenon lamp, showing the laser diode with narrow bandwidth, the LED with relatively wide bandwidth and xenon with very broad bandwidth, and (b) the focus lens and emission filter. (c) A plot of signal-to-noise ratio (SNR) *vs* contrast for different charge-coupled device (CCD)-based detectors with integration time of 200 ms. Both front-illuminated intensified CCD (FICCD) and back-illuminated intensified CCD (BICCD) are superior to the other types of CCD cameras (Zhu et al[25]). BCCD, back-illuminated CCD; EMCCD, electron-multiplying CCD; FCCD, front-illuminated CCD; OD, optical density.

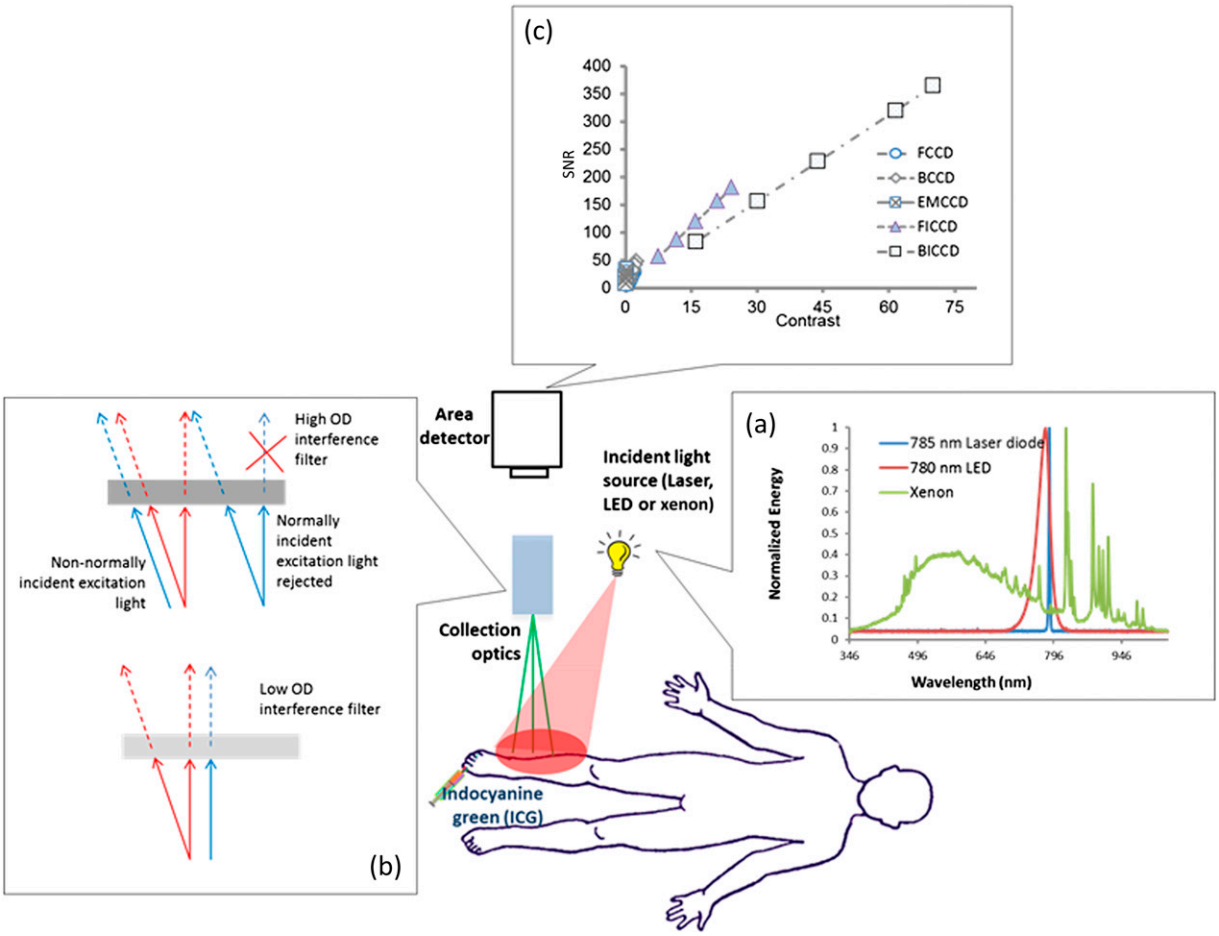

is $0.2 \times 10^{2(\lambda - 0.700)}$ W cm^{-2} (where the wavelength λ is reported in units of micrometre). For 785 nm, the limit for eye safety is 1.48 mW cm^{-2} and for skin safety is 296 mW cm^{-2}. As shown in Table 1, all laser-based devices used in clinical studies probably exceed MPE for eye safety but not for skin safety. It should be noted that devices that exceed the MPE require the use of eye protection for the patient, and precautions for the healthcare personnel. In addition, with greater excitation incident power, there is greater backscattered light, which, as discussed in the next section, can contribute to obtain a high background, obscure collection of weak ICG signals and limit device performance.

Collection optics

Without exception, all ICG fluorescence imaging systems have detection sensitivities that are limited by background signals (or noise floor) that arise from one or more of the following: (i) the spectral overlap between the backscattered excitation light and collected ICG fluorescence allowing non-fluorescent signals to be registered as fluorescence; (ii) a "blue shifting" of optical filters that allows passage of non-collimated, backscattered excitation light not normally incident on the filter surface, and (iii) the limited optical density of optical filters that allows passage of a small amount of ambient and excitation light that is still significant compared with the weak, collected ICG fluorescence (Figure 1b).[26] If light that does not originate from the fluorescent dye resident in the tissues is collected, then it represents the "noise floor" making it less probable that the device can image small quantities of a NIRF agent in tissues.

It is also important to note that the sensitivity of the fluorescent imaging device can also be impacted in the environment in which it is used. While it is not feasible to work in total darkness, variation in ambient light, whether provided by fluorescent or incandescent room lighting, surgical lamps or white light illumination in endoscopy or laparoscopic devices, can have small but significant spectral contributions within the spectral bandwidths in which ICG fluorescence is collected.

Area detectors

Currently, charge-coupled device (CCD) detectors are primarily used in ICG fluorescence imaging systems and depend upon integrating the collected photons over millisecond time frames. The CCD detectors used can be divided into (i) front- and back-illuminated CCDs (FCCDs and BCCDs), (ii) electron-multiplying CCDs (EMCCDs) and (iv) intensified CCDs (ICCD), including front- and back- illuminated ICCD based on their configurations. Most imaging systems employed in humans use either FCCD or BCCDs (Table 1). FCCDs are constructed in a fashion similar to the human eye by orienting polysilicon gates at the front, wiring in the middle and photodiodes for light collection at the back. This configuration blocks incident light from reaching the photodiodes resulting in relatively low QE. BCCDs contain the same elements, but by rearranging the gate structure to the back of the photosensitive area of the CCDs and by reducing the thickness of the silicon layer via proprietary etching techniques, BCCDs have more than two-fold improvement in QE than do their front-illuminated counterparts. Unlike a conventional CCD, an EMCCD has an additional electron-emitting register installed between the normal serial register and the output amplifier to multiply weak signals. The EM register is split up into several hundred stages, and each stage acts as an avalanche diode to multiply the signal. The degree of multiplication gain can be controlled by varying the clock voltages applied to the EM register.

By contrast, ICCDs have a different multiplication mechanism, in which an image intensifier amplifies the collected image before it is registered by a CCD. The intensifier consists of three main components, a photocathode, an EM microchannel plate (MCP) and a phosphor screen. The photocathode coverts the low level of incoming light into electrons, which are then accelerated and amplified by a high electrical field towards the MCP and, finally, the amplified signal is converted back into a light signal at the phosphor screen ready for the CCD acquisition. In NIR sensitive generation III intensifiers, a thin film of sintered aluminium oxide is attached to the MCP to protect the photocathode from spurious backscattered ions. Generation II intensifiers are more common but lack the sensitivity to NIR light of generation III intensifiers.

The potential noise sources in these CCD devices consist of the signal inherent shot noise, dark current noise and readout noise.[27] Shot noise results from the inherent statistical fluctuations in the number of photons incident on the CCD and represents the detection limit of a detector. For the ICCDs and EMCCDs, shot noise is a function of the mean incident photon flux, multiplication gain, QEs, integration time and a noise factor that characterizes the noise introduced by the gain process. Dark current noise arises from statistical variation in the number of thermally generated electrons that accumulate in the pixels of all CCDs. The rate of dark current generation highly depends on the temperature of the CCD and is especially important for EMCCDs, since it is multiplied by the on-chip multiplication gain. For the ICCDs, additional dark current noise is generated by spontaneous electron output from the intensifier photocathode and is magnified by the multiplication gain of the intensifier. Cooling the CCD can reduce the dark current noise to a negligible level over a typical exposure interval in high-performance CCD cameras. Readout noise is a combination of system noise components inherent to the process of converting CCD charge carriers into an analogue voltage signal for quantification, and the subsequent analogue-to-digital (A/D) converter that converts the analogue voltage signal into a digital representation. For EMCCDs, the readout noise consists of two components: the charge transfer noise arising from the multiplication effect of gain register and all other non-multiplied readout noises. Readout noise becomes dominant in conventional CCDs operating at high frame readout frequency. Our studies showed that the imaging performance of generation III ICCD systems is superior and better than that of unintensified CCD systems in both signal-to-noise ratio and target-to-background ratio when the integration time of CCD camera is $<$200 ms,[25] as shown in Figure 1c. This performance may be expected owing to the optimal amplification of the collected NIRF signal by the intensifier and the subsequent integration that reduces the amplified noise. In general, increased integration times result in maximum signal and reduced noise levels, but at long integration times, motion artefacts and camera saturation owing to limited dynamic range can result. Dynamic range of CCD-based measurements is limited by the A/D register and is typically 8, 10, 12 or the maximum dynamic range of 16-bits.

Investigational and marketed near-infrared fluorescence imaging devices

Several investigational and market NIRF imaging devices have been used clinically (Table 1) and can be divided into the following classifications: (i) hand-held [including HyperEye Medical System (Mizuho Medical), FLUOBEAM® (Fluoptics, Grenoble, France), PDE (Hammatsu Photonics Co., Hamamatsu, Japan), IC-View (Pulsion Medical Systems SE, Feldkirchen, Germany) and Visual Navigator (SH System, Seoul, Republic of Korea)], (ii) cart-based (including FDPM imager, mini-FLARE, SPY and the Prototype Surgical Navigation System) and (iii) incorporated into existing devices, such as the da Vinci® Robotics System (Novadaq Technologies Inc.), by the incorporation of NIR illumination and detection capability (including INFRARED™ 800™, FIREFLY™ and laparoscopic NIRF system). Figure 2 are the photos of typical investigational (FDPM imager) and marketed (PDE and SPY) NIRF imaging devices. The fluence rate of fluorescence excitation light source varies among these systems with the range of $<$1.9–31 mW cm^{-2}. The fluorescence excitation wavelengths are also different in these systems. For example, FLUOBEAM, FDPM imager, SPY and FIREFLY employ laser didoes operating at 750, 785 and 806 nm, respectively. mini-FLARE, PDE, HyperEye Medical System and Visual Navigator employ LEDs with a centred wavelength located at 760 or 740 nm. INFRARED 800 and FIREFLY utilize the filtered xenon with wavelengths ranging from 700 to 800 nm. The CCD cameras in these systems have varying dynamic ranges and integration times that vary from 0.1 to 1000.0 ms. Collection wavelengths in these systems are mainly centred at 830 nm, which is close to the emission peak of ICG fluorophore and at which CCD cameras have moderately high

Figure 2. Photos of typical investigational and marketed near-infrared fluorescence imaging devices: (a) FDPM imager (University of Texas Health Science Center at Houston, TX), (b) Photodynamic eye (PDE; Hamamatsu Photonics Co., Hamamatsu, Japan) and (c) SPY (Novadaq Technologies Inc., Toronto, ON, Canada).

(a) (b) (c)

sensitivity. Some systems such as SPY and PDE have fixed working distance (WD) of 30 and 20 cm, respectively, and fixed fields of view (FOVs) of 19×12.7 and 10×6.7 cm^2, respectively. In these systems, the proper WD is found by positioning the camera head until there is a superposition of two points of LED illumination on the tissue surface to be imaged. Other systems such as the FDPM imager, mini-FLARE and FLUOBEAM have adjustable WDs and FOVs. To accommodate various surgical applications, some systems (including FDPM imager and mini-FLARE) are designed with adjustable WD and FOV accomplished through manual or automatic focus lens along with a moveable articulating arm. During intraoperative or non-invasive applications, it is important to correlate the collected fluorescent image to the actual FOV either by (1) collecting light from a single view in one optical path and spectrally separating the "white-light" and "fluorescent" images for collection by different detectors for direct overlay on display or by (2) collecting two different "white-light" and fluorescent views and co-registering the separate views for combined display.

As depicted in Table 1, the WD, FOV, wavelength specifications for excitation illumination and fluorescence collection, and, finally, detector type varies widely among the devices used in clinical studies. Because the variation in instrument design could result in variable performance, one might expect that varying amounts of ICG employed in these clinical studies could be used to infer performance in lieu of the missing standardized measurements and specification of performance as discussed above. Secondly, NIRF imaging provides an unmet clinical need to assess the lymphatic vasculature and its function.[18,19] For these two reasons, we focus upon the clinical application of these devices in which the lymphatic vasculature is interrogated with varying amounts of ICG, whether for identification of SLNs for cancer staging or for assessment of the lymphatic vasculature for diagnosis of various conditions or diseases.

INDOCYANINE GREEN IMAGING OF LYMPH NODES FOR CANCER STAGING

Lymph node mapping for identification of tumour draining lymph nodes for resection and subsequent pathological application in many cancers is commonly performed intraoperatively using blue dyes and/or transcutaneously and intraoperatively with non-specific technetium-99m (^{99m}Tc) radiocolloid. While emerging technologies employ i.v. administration of ultrasmall superparamagnetic iron oxide particles[28] and intradermally administered radiolabelled mannose sugar, tilmanocept[29], intradermal and subcutaneous administration of ICG to locate draining lymph nodes represents an emerging area in nodal staging. The primary advantages of using a radiolabelled fluorescent molecule or NIR active compound is the direct relationship between the regions of fluorescence emitted from tissue surfaces within the surgical FOV. Lymph node detection is often achieved intraoperatively using a gamma probe to provide an audible signal when placed transcutaneously or over a small tissue region containing radioactivity within the surgical FOV. The gamma probe enables localization but does not provide sufficient boundary discrimination to finely guide surgical resection. The advantage for using an NIR fluorescent agent such as ICG over a blue intravital dye is the opportunity to detect subsurface lymph nodes or tissues that may not otherwise be detected intraoperatively within the surgeon's FOV. While ICG fluorescence remains limited in tissue penetration, diagnostic nuclear imaging remains the hallmark for assessing tumour-draining deep lymph nodes in a pre-operative fashion. As a result, in the majority of studies using ICG fluorescence navigation for localizing tumour draining lymph nodes, it is used intraoperatively, rather than non-invasively, in a pre-operative setting as reviewed by Vahrmeijer et al.[23] It is important to note that because ICG is not cancer specific, it cannot be used for NIRF detection of cancer-positive lymph nodes, which is the goal of emerging NIRF molecular imaging agents.[30–32] A recent review of NIRF molecular imaging agents for identification of tumour margins during cancer surgery is not contained herein but rather in Vahrmeijer et al.[23] The following sections detail the performance of the various devices used intraoperatively for SLN detection.

Sentinel lymph node mapping in breast cancer

The majority of studies using ICG fluorescence imaging for lymph node detection are performed in breast cancer as summarized in Table 2. Kitai et al[33] first utilized the fluorescence properties of ICG for SLN detection in patients with early breast

Table 2. Summary of sentinel lymph node (SLN) detection in breast cancer patients

Study	Number of subjects	Mean age of subjects (years)	Total dose of ICG	Injection site	Device	Operative time (min)	Averaged number of SLNs	Detection rate (%)	Comments
Kitai et al[33]	18	56.9	25 mg in 5 ml	Subcutaneous periareolar	Prototype of PDE	<30	2.8 (1–6)	17/18 (94)	The use of prototype PDE for SLN detection
Tagaya et al[34]	25	–	5 mg in 1 ml	Subdermal periareolar	PDE	15 (8–25)	5.5 (3–10)	100	ICG is superior to blue dye with a larger number of SLNs detected
Sevick-Muraca[1]	24	57.7 (30–85)	0.00031–0.1 mg in 0.1–3.0 ml	Periareolar and deep peritumour	FDPM imager	Immediately	1.7 (dose >10 μg)	87 (dose >10 μg)	Determine the minimum dose needed for visualization of lymph drainage pathways
Murawa et al[35]	30	56 (27–84)	5 mg in 1 ml, 10 mg in 2 ml, 15 mg in 3 ml	Intradermal periareolar	IC-View	5–10	1.75	29/30 (97)	Visualization of lymphatic vessels depends on the different doses of ICG. ICG is superior to radioisotope
Troyan et al[36]	6	61 (51–65)	0.0124 mg in 1.6 ml	Peritumour	Mini-FLARE™	5	1.5 (1–4)	9/10	The use of ICG: HSA detected by mini-FLARE
Sugie et al[37]	411	57.9 (30–91)	5 mg in 1 ml	Periareolar	PDE	–	2.3 (1–9)	408/411 (99)	ICG is superior to blue dye
Hirche et al[38]	43	58.4 (27–83)	11 mg in 2.2 ml	Subareolar	IC-View	5–15	2.0 (1–3)	42/43 (98)	–
Hojo et al[39]	141	57.6 (34–83)	10 mg in 2 ml	Intradermal peritumour and subareolar	PDE	>5	3.8	140/141 (99)	Comparison of ICG, patent blue and radioisotope. The combination of ICG and blue dye is a highly sensitive method
Tagaya et al[40]	50	–	1.25 mg in 0.5 ml	Subdermal areola	PDE	10.3 (6–18)	3.7 (1–7)	100	With additional imaging overly navigation system

(Continued)

Table 2. (Continued)

Study	Number of subjects	Mean age of subjects (years)	Total dose of ICG	Injection site	Device	Operative time (min)	Averaged number of SLNs	Detection rate (%)	Comments
Mieog et al[41]	24	59.5 (33–81)	0.062–1.24 mg in 1.6 ml	Peritumour or periareolar	Mini-FLARE	16 ± 3	1.43 (1–3)	100	Optimal injection dose of ICG:HSA ranged between 0.062 and 1.240 mg per 1.6 ml^{-1} validated on mini-FLARE
Hutteman et al[42]	18	59.5 (38–72) and 57.5 (40–73)	0.62 mg in 1.6 ml	Four intradermal four periareolar	Mini-FLARE	15.6 ± 2.2	1.4 ± 0.5	100	Comparison of ICG:HSA with ICG alone, showing no difference in SLN identification rate
Abe et al[43]	128	53 (29–73)	0.75 mg in 0.15 ml	Intradermal	PDE	<15	3.1 (1–6)	100	ICG fluorescence demonstrated higher sensitivity compared with that of blue dye
Aoyama et al[44]	312	57.4 (29–85)	0.625 mg in 5 ml	Subareolar periareolar	PDE	A few	3.41 (1–12)	100	–
van der Vorst et al[45]	24	59 (39–75)	0.62 mg in 1.6 ml	Four intradermal four periareolar	Mini-FLARE	15.2 ± 3.0	1.5 ± 0.8 (1–4)	23/24 (96)	No benefit of using patent blue when combining ICG with radioisotope
Wishart et al[46]	100	60 (34–81)	10 mg in 2 ml	Intradermal and subcutaneous-periareolar	PDE	–	1.93 (1–5)	100	Comparison of ICG, blue dye and radioisotope. The combination of ICG and blue dye had the highest nodal sensitivity method, avoiding the need of the radioisotope method

(Continued)

Table 2. (Continued)

Study	Number of subjects	Mean age of subjects (years)	Total dose of ICG	Injection site	Device	Operative time (min)	Averaged number of SLNs	Detection rate (%)	Comments
Hirano et al[47]	108	60.5 (31–85)	5 mg in 2.5 ml	Subareolar	PDE	–	2.2 (1–5)	100	The combination of blue dye with ICG is superior to blue dye alone
Takeuchi et al[48]	145	57.2 (30–83)	5 mg in 1 ml	Subcutaneous periareolar	PDE	–	–	144/145 (99)	–
Polom et al[49]	49	54.4 (31–71)	0.465–10 mg in 1 ml	Intradermal	PDE	–	–	47/49 (96)	–
Sugie et al[50]	99	60 (29–75)	2.5–5.0 mg in 0.5–1.0 ml	Subareolar	PDE	–	3.4 (1–7)	98/99 (99)	ICG is superior to blue dye
Schaafsma et al[51]	32	56 (34–82)	0.05 mg in 0.2 ml	Periareolar	Mini-FLARE	24 h (19–29)	1 (1–2)	100	Integration of ICG and radioactive labels in a single tracer
Jung et al[52]	43	48.2 ± 9.6	0.18 mg in 0.3 ml	Subareolar	Visual Navigator	6.5 ± 5.2	3.4 ± 1.4	100	A mixture of ICG, radioisotope and blue dye compared with radioisotope alone, high number SLNs detected by the mixture method
Guo et al[53]	36	55.2 (30–81)	5 mg in 1 ml	Subareolar	PDE	5–10	3.6	35/36 (97)	ICG is superior to blue dye
Chi et al[54]	22	49 (32–68)	1–2 mg in 0.2–0.4 ml	Subcutaneous areolar	The prototype surgical navigation system	5–10	2.7 (1–6)	100	Use of a prototype surgical navigation system for SLN detection
Ballardini et al[55]	134	–	5 mg in 1 ml	Subdermally, peritumoural	PDE	–	–	99.6	Concordance between ICG and radiotracer methods. ICG and NIRF imaging can be used with equal success of the radiotracer method to detect SLNs

(Continued)

Table 2. (Continued)

Study	Number of subjects	Mean age of subjects (years)	Total dose of ICG	Injection site	Device	Operative time (min)	Averaged number of SLNs	Detection rate (%)	Comments
Verbeek et al[56]	95	57 (30–75)	0.62 mg in 1.6 ml	Intradermal periareolar or peritumour	Mini-FLARE	19 ± 7.1	1.9 (1–5)	94/95 (99)	The comparison of ICG, radioisotope and blue dye; call for a standard method

HSA, human serum albumin; ICG, indocyanine green; NIRF, near-infrared fluorescence; PDE, photodynamic eye.
The devices mentioned in the table and their manufacturer details in parenthesis are as follows: FDPM imager (University of Texas Health Science Center at Houston, TX), IC-View (Pulsion Medical Systems SE, Feldkirchen, Germany), Mini-FLARE (Israel Beth Deaconess Medical Center, Boston, MA), PDE (Hamamatsu Photonics Co., Hamamatsu, Japan) and Visual Navigator (SH System, Seoul, Republic of Korea).

cancer using the PDE prototype device using 25 mg of ICG in 5 ml of water. Intraoperatively, sentinel nodes were found by visually following the green-stained lymphatic vessels to the first-draining SLNs that were fluorescent. Since then, comparative studies have been performed to assess performance of ICG, blue dye and radioisotope alone or in combination using a range of devices and ICG doses.[34–38,40,43–50,52–56] In general, reports are mixed but show that fluorescence imaging provides higher detection rate and lower false-negative rate than do blue dye and radioisotope methods,[34,35,37,50,53] and the combination of fluorescence imaging with blue dye visualization was found to be superior to the blue dye method alone.[39,47] Moreover, the combination of fluorescence imaging with blue dye visualization had the highest sensitivity method, avoiding the need of the radioisotope method,[46] and in another study, no benefit was found in using the blue dye when ICG was combined with radioisotope method.[45] Investigators who used the mini-FLARE device often combined ICG with human serum albumin (HSA) to improve quantum yield and SLN retention of ICG fluorophore.[36,41,42] Addition of HSA to ICG was not found to significantly alter SLN detection rate when the PDE device was used for detection.[42] In another study of 134 patients with breast cancer, detection of SLNs from ICG was not found to be superior to the radiotracer method using the PDE device.[55] Combination of ICG and radiotracer has also been attempted for NIRF and gamma detection of SLNs in breast cancer,[51] enabling preoperative localization from nuclear imaging and intraoperative guidance from NIRF imaging, but earlier studies showed that ICG was especially unstable and lost its fluorescent properties when mixed with the acidic solutions used to suspend and administer ^{99m}Tc radiocolloid.[1,57] To date, various total doses of ICG, ranging from as little as 10 μg by Sevick-Muraca et al,[1] to as much as 25 mg used by Kitai et al,[33] have been successfully injected for non-invasive and intraoperative detection of visualization of lymph drainage pathways and SLNs. Mieog et al[41] determined that the optimal total dose of ICG detected using the mini-FLARE device lies between 0.062 and 1.240 mg of ICG in 1.6 ml of total injection volume. The injection sites of ICG fluorophore have been intradermal periareolar, subcutaneous periareolar, subareolar and deep tumour or a combination thereof, but there is no evidence showing that the SLN detection rate from ICG is affected by intradermal *vs* subcutaneous route of administration. However, because ICG is non-specific, there is a chance that ICG may drain from the injection sites and receiving lymph node basins prior to detection, resulting in false-negative SLN detection. A typical ICG fluorescence-guided SLN harvesting in a patient with breast cancer using the mini-FLARE device is shown in Figure 3. The number of detected SLNs reported in different clinical studies using ICG fluorescence imaging is variable but, generally, is reported to have higher detection rates than do conventional methods.

Skin cancer

Studies using ICG fluorescence imaging for SLN detection in skin cancer are summarized in Table 3. Fujiwara et al[58] first reported the use of fluorescence method to identify the SLN successfully in melanoma and squamous cell carcinoma of the

Figure 3. Single sentinel lymph node (SLN) identified and resected for a patient with breast cancer after injection (Inj.) of indocyanine green. Colour video images are shown in the left, near-infrared (NIR) fluorescence imaging is shown in the middle and a pseudocoloured merge of the two are shown in the right, where arrows point to the positions of the SLN. LC, lymphatic channel. Reproduced from Troyan et al[36] with permission from Springer Science + Business Media.

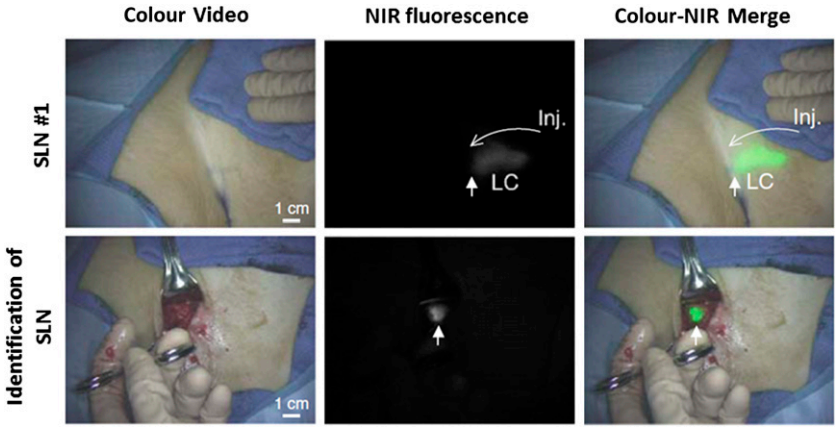

skin. Moreover, they found that use of fluorescence method avoids the "shine-through" phenomenon seen in lymphoscintigraphy, thereby providing high detection rate of the cervical SLN.[64] In general, 0.5 mg in 0.1 ml dose of ICG was injected intradermally at various sites around the tumour, with a total dose volume ranging from 0.4 to 1.0 ml. To improve fluorescence signal, ICG:HSA was also used in melanoma SLN detection,[69] and the ICG:HSA dose escalation clinical trial was also performed.[71] In addition, the effectiveness and limitations of fluorescence detection of lymph nodes were evaluated with transcutaneous imaging, and imaging within the surgical FOV and of the excised tissues. Studies showed a lower detection of lymph nodes from transcutaneous as opposed to from within the surgical FOV or from resected tissues containing lymph nodes.[70] It was observed that transcutaneous SLN detection rate could be improved by manual manipulation of overlying tissues or by increasing the dose of ICG.[70] Other opportunities for improving detection could result from improving device sensitivity.

Other cancers

Studies using ICG fluorescence imaging for SLN detection in other cancers are summarized in Table 4. Miyashiro et al[73] used the fluorescence method to detect the SLN of gastric cancer in open gastrectomy, and ICG was injected endoscopically around the tumour 1 day before surgery. Later studies showed that pre-operative, endoscopic ICG injection provides a larger averaged number of SLNs, a higher accuracy rate and a lower false-negative rate than does intraoperative ICG injection in cT1-stage gastric cancer.[74] Some investigators showed the possibility of SLN mapping guided by ICG fluorescence imaging during laparoscopy-assisted gastrectomy.[75] The adequate dose of ICG injected submucosally on the day before operation has been reported to be four doses of 0.5 ml containing 50 μg in 1 ml ICG for SLN mapping using HyperEye Medical System in the gastric cancer surgery.[77] The NIRF method has also been applied for SLN mapping in rectal,[79] anal,[80] colon[78,81] and colorectal[82] cancers with acceptable detection rates. Moreover, the SLN could be detected not only in T1 disease but also in T2 and T3 disease.[79] In these studies, the total dose of ICG ranged from 14 mg in 2.8 ml to 25 mg in 5 ml injected around the tumours. The da Vinci, integrated with FIREFLY, has been used for SNL mapping in bladder and prostate cancer.[83,84] Recently, the application of the NIRF method for SLN detection was attempted in cervical cancer,[85,86] showing a similar detection rate as that using the blue dye and radioisotope method. As in breast and skin cancers, 1.6 ml of ICG:HSA was injected around the tumour for SLN mapping in patients with cervical cancer.[87] Further studies demonstrated that there is no advantage of ICG:HSA over ICG alone for SLN detection in early stage cervical cancer, thus avoiding the added cost and complexity in using ICG:HSA.[89] SLN mapping has also been demonstrated using robotically assisted endoscopic NIR imaging after cervical injection of appropriate dose of ICG around the tumour.[88] The NIRF method for SLN mapping has been introduced in other types of cancers, such as vulvar and endometrial cancer,[90–94] head and neck cancer[95–97] and non-small-cell lung cancer[98,99] with high detection rate.

In the Western world, the incurable condition of lymphoedema is generally caused after both SLN and full lymph node resections, presenting without warning weeks to years after surgery. Although lymphoscintigraphy has been performed routinely to image the lymphatics, the long integration times and relatively low spatial resolution of this technique limit its application for real-time imaging of lymphatic contractile function and for visualizing fine lymphatic architecture. Recently, ICG fluorescence imaging has been adopted for human lymphatic imaging, as described in the following section.

LYMPHATIC IMAGING

Clinical lymphatic imaging studies using NIRF imaging systems are summarized in Table 5. NIRF imaging has been used to characterize lymphoedema of the upper and lower extremities using both PDE[2,16,20,100–104,107–113,116,117,119,120,122] and FDPM devices.[1,22,105,106,114,118,121] Interpretation of NIRF images include aberrant lymphatic vasculature as seen comparatively to

Table 3. Summary of sentinel lymph node (SLN) detection in patients with skin cancer

Study	Number of subjects	Mean age of subjects (years)	Total dose of ICG	Injection site	Device	Operative time (min)	Averaged number of SLNs	Detection rate (%)	Comments
Fujiwara et al[58]	10	68 (34–80)	3–5 mg in 0.6–1.0 ml	Intradermal peritumour	PDE	<15	–	–	The detection of the SLN in melanoma and squamous cell carcinoma of the skin: the first report
Tsujino et al[59]	2	75, 88	5 mg in 1 ml	Intradermal	PDE	2–3	–	–	–
Tanaka et al[60]	6	–	5–8 mg in 1 ml	Intradermal	PDE	–	–	100	ICG fluorescence is superior to the blue dye method
Mizukami et al[61]	24	–	3–10 mg in 0.6–2.0 ml	Intradermal	PDE	–	–	23/24 (96)	–
Namikawa et al[62]	49	62 (18–85)	5 mg in 1 ml	Intradermal peritumour	PDE	Approximately minutes	4.0	61.1, 100	A combination of blue dye, radioisotope and fluorescence method for improving SLN detection rate
Fujisawa et al[63]	16	–	1.5 mg in 0.3 ml to 3.0 mg in 0.6 ml	Intradermal peritumour	FNS	10	1.5 per basin (1–3)	100	A custom-made low-cost intraoperative system developed and tested
Hayashi et al[64]	1	47	2 mg in 0.4 ml	Intradermal peritumour	PDE	–	–	100	Fluorescence method overcomes the shine-through phenomenon in head and neck/lip mucosa melanomas
Stoffels et al[65]	22	51.63	0.2 mg in 1 ml	Peritumour	PDE	5–10	2.8	100	Fluorescence method is an attractive option with radioisotope method
Fujisawa et al[67]	34	–	2.0 mg in 0.4 ml to 4.0 mg in 0.8 ml	Intradermal peritumour	–	<15	2.18	100	Fluorescence method is superior to the conventional methods

(Continued)

Table 3. (Continued)

Study	Number of subjects	Mean age of subjects (years)	Total dose of ICG	Injection site	Device	Operative time (min)	Averaged number of SLNs	Detection rate (%)	Comments
Rasmussen et al[68]	4	–	0.4 mg in 1.6 ml	Peritumour, intradermal	FDPM imager	–	–	–	Study assessed tumour draining lymphatics longitudinally in patients with cancer but did not assess surgically guided resection of SLN
Polom et al[66]	10	56.4 (26–79)	0.2–0.93 mg in 2 ml	Peritumoural, intradermal	PDE	–	1.9	–	Radioisotope and ICG methods yield the same results
van der Vorst et al[69]	15	55 (21–70)	0.75, 1.0, 1.2 and 1.5 mg in 1.6 ml	Peritumour	Mini-FLARE™	12.6 ± 3.6	2.0 ± 1.6	93	An ICG:HSA concentration of 0.744 mg per 1.6 ml appears optimal with mini-FLARE
Namikawa et al[70]	86	63 (18–87)	2.0 mg in 0.4 ml to 5.0 mg in 1.0 ml	Intradermal peritumour	PDE	–	–	63.4, 98.9, 100	The evaluation of the SLN detection rate at the "before skin incision", "after skin incision" and "*ex vivo*" surgical stages
Gilmore et al[71]	25	47 (25–79)	77.5, 193.8 or 387.5 μg in 1.0 ml	Intradermal peritumour	Mini-FLARE	>5	2.6	24/25 (96)	The dose escalation clinical trial
Nakamura et al[72]	12	66 (32–85)	3.0 mg in 0.6 ml	Intradermal peritumour	–	–	3.2	95	The improvement in the detection rate of cervical sentinel nodes in head and neck skin cancer using fluorescence method in combination with the standard technique

FNS, fluorescence navigation system; HSA, human serum albumin; ICG, indocyanine green; PDE, photodynamic eye.
The devices mentioned in the table and their manufacturer details in parenthesis are as follows: FNS (University of Tsukuba, Tsukuba, Japan), PDE (Hamamatsu Photonics Co., Hamamatsu, Japan), FDPM imager (University of Texas Health Science Center at Houston, TX), Mini-FLARE (Israel Beth Deaconess Medical Center, Boston, MA).

Table 4. Summary of sentinel lymph node (SLN) detection in other patients with cancer

Study	Type of cancer	Number of subjects	Mean age of subjects (years)	Total dose of ICG	Injection site	Device	Operative time (min)	Averaged number of SLNs	Detection rate (%)	Comments
Miyashiro et al[73]	Gastric cancer	3	66 (60, 66, 73)	10–20 mg in 2–4 ml	Peritumour	PDE	A few and 1 day	3 (4, 1, 4)	100	ICG injected 1 day before surgery
Tajima et al[74]		56	68.4 ± 10.1	10 mg in 2 ml	Submucosa peritumour or into subserosa	PDE	A few or 1–3 days	7.2 ± 7.0 (1–30)	54/56 (96)	Pre-operative injection of ICG is preferable with cT1 stage cancer
Tajima et al[75]		77	67.2 ± 10.6	10 mg in 2 ml	Submucosa peritumour or subserosa	PDE-2	1–3 days	7.9 (LAG) 7.2 (OG)	94.7, 94.9	SLN mapping possible, even during LAG
Miyashiro et al[76]		10	68 ± 8 (54–79)	1–10 mg in 2–4 ml	Peritumour	A prototype laparoscopy	Approximately 5	3.1 ± 1.5 (1–6)	100	Development of a prototype laparoscopic system for SLN detection in gastric cancer
Yoshida et al[77]		12	58.4 ± 14.3	0.05–0.2 mg in 2 ml	Submucosal peritumour	HyperEye Medical System	1 day	3.6 ± 2.1	100	Determination of ICG dose and harvesting time
Watanabe et al[78]	Rectal, anal, colon, colorectal bladder cancer	10	62.5 (43–80)	5 mg in 2 ml	Submucosa	PDE	–	–	100	Detection of tumour
Noura et al[79]		25	58.4 ± 11.6 (33–74)	5 mg in 1 ml	Peritumour	PDE	<30	2.1 ± 0.8 (1–4)	23/25 (92)	Detection of lateral SLN not only in T1 and T1 diseases, but also in T3 diseases
Hirche et al[80]		12	58 (21–90)	25 mg in 5 ml	Subdermal peritumour	IC-View	10–15	1.6	10/12 (83)	Application in anal cancer
Hirche et al[81]		26	67 (46–87)	5–20 mg in 1–4 ml	Peritumour	IC-View	3–10	1.7 (0–5)	25/26 (96)	The application in colon cancer
Cahill et al[82]		18	66 (48–80)	10–15 mg in 1–3 ml	Submucosal peritumour	Laparoscopic NIRF system	1 day (1 case), 10	12 (1 day) and 3.6 (1–5)	100	Use of NIR laparoscopy for SLN detection in early stage colorectal neoplasia

(Continued)

Table 4. (Continued)

Study	Type of cancer	Number of subjects	Mean age of subjects (years)	Total dose of ICG	Injection site	Device	Operative time (min)	Averaged number of SLNs	Detection rate (%)	Comments
Manny and Hemal[83]	Prostate cancer	10	71 (54–77)	5 mg in 2 ml	Peritumour	FIREFLY™ (da Vinci®)	30	16 (12–25)	100	Using the combined cystoscopic and intravenous injection of ICG in bladder cancer
Manny et al[84]		50	66 (51–73)	1 mg in 0.4 ml	The lobe of the prostate	FIREFLY (da Vinci)	30	–	100	Application in prostate cancer
Furukawa et al[85]	Cervical, vulvar, endometrial cancer	12	58 (36–68)	4 mg in 0.8 ml	In the cervix	PDE	30 (20–40)	7 (3–10)	10/12 (83)	Fluorescence method comparable with the conventional method
Crane et al[86]		20	51.3 (39–74)	0.5 mg in 1 ml	In the cervix	Custom	0.5	1.5	6/9 (67)	–
van der Vorst et al[87]		9	40 (29–77)	0.62, 0.93 or 1.24 mg in 1.6 ml	Transvaginal submucosal peritumour	Mini-FLARE™	51 ± 18	3.4 ± 1.2 (1–5)	100	The optimal concentration of ICG: HSA is 0.62 mg in 1.6 ml with Mini-FLARE
Rossi et al[88]		20	61 (28–82)	1 mg in 2 ml	1 cm into the cervical stroma	SPY	37.3 (8–60)	4.5 (0–9)	85	Appropriate dose required with robotic assistance
Schaafsma et al[89]		18	40 (28–67)	0.62 mg in 1.6 ml	Submucosal peritumour	Mini-FLARE	43 ± 14	2.9 (ICG: HSA) 2.7 (ICG)	14/18 (78)	No advantage of ICG: HSA over ICG alone for the SLN detection in early stage cervical cancer
Crane et al[90]		10	67.5 (46–82)	0.5 mg in 1 ml	Peritumour	Custom	Immediately	2.6 (1–6)	100	Transcutanous SLN mapping possible in 50% of all patients
Hutteman et al[91]		9	50 (30–72)	0.62–1.24 mg in 1.6 ml	Peritumoural	Mini-FLARE	19 ± 4	1.6 (1–4)	100	ICG:HSA solution used
Holloway et al[92]		35	63.4	2.5 mg in 2 ml	Injected into cervix	FIREFLY (da Vinci)	10	–	100	Robotic-assisted lymphadenectomy

(Continued)

Table 4. (Continued)

Study	Type of cancer	Number of subjects	Mean age of subjects (years)	Total dose of ICG	Injection site	Device	Operative time (min)	Averaged number of SLNs	Detection rate (%)	Comments
Rossi et al[93]		29	62 63.5	0.5–1.0 mg	Cervical ($n = 17$) and hysteroscopic injections ($n = 12$)	FIREFLY (da Vinci) or SPY	–	5 (1–9) 2.5 (1–3)	82% for cervical injection 33% for hysteroscopic	A higher SLN detection rate by cervical injection compared with hysteroscopic endometrial injection
Jewell et al[94]		227	60 (28–90)	5 mg in 4 ml	Into cervix, stroma and submucosa	FIREFLY (da Vinci)	–	3 (1–23)	216/227 (95)	Blue dye appears unnecessary
Bredell[95]	Head and neck cancer	8	–	10 mg in 1 ml	Peritumour	PDE	5	3 (1–5)	100	–
van den Berg et al[96]		14	65.5 (51–84)	0.05 mg in 0.4 ml	Peritumour	PDE	10	3.4 (1–7)	100	ICG can detect SLNs located in close proximity to the primary tumour
van der Vorst et al [97]		10	59.5 (33–73)	0.62 mg in 1.6 ml	Peritumour	Mini-FLARE	5–30	1.7 ± 0.8	100	–
Yamashita et al[98]	Non-small-cell lung cancer	31	63 (54–83)	10 mg in 2 ml	Peritumour	Infrared Camera Systems	10	1.3–1.4	25/31 (81)	–
Gilmore et al[99]		38	64.9 ± 10.3	0.0038–2.5 mg	Peritumour	Mini-FLARE/ and Novadaq® NIR camera	5	1.7	90 at the dose of ICG >1 mg	Identification of optimized dose of ICG

HSA, human serum albumin; ICG, indocyanine green; LAG, laparoscopy-assisted gastrectomy; NIRF, near-infrared fluorescence; OG, open gastrectomy; PDE, photodynamic eye.
The devices mentioned in the table and their manufacturer details in parenthesis are as follows: FIREFLY (da Vinci; Novadaq Technologies Inc., Toronto, ON, Canada), HyperEye Medical Systems (Mizuho Medical Co., Ltd, Tokyo, Japan), IC-View (Pulsion Medical Systems SE, Feldkirchen, Germany), Infrared Camera Systems (Olympus, Tokyo, Japan), Mini-FLARE (Israel Beth Deaconess Medical Center, Boston, MA), Novadaq NIR camera (Novadaq Technologies Inc.), PDE (Hamamatsu Photonics Co., Hamamatsu, Japan), SPY scope (Novadaq Technologies Inc.).

Table 5. Summary of lymphatic imaging using indocyanine green (ICG) fluorophore

Study	Number of subjects	Total dose of ICG	Injection site	Device	Comments
Unno et al[100]	22	2 mg in 0.4 ml	Subcutaneously at the dorsum of the foot	PDE	The first published report of ICG fluorescence imaging of human lymphatics in lymphoedema and normal subjects
Ogata et al[16]	5	2 mg in 0.4 ml	Intracutaneously into the dorsal aspect of foot (first web space)	PDE	Guiding lymphaticovenular anastomoses
Unno et al[2]	10	3 mg in 0.6 ml	Subcutaneously at the dorsum of the foot	PDE	Quantitation of lymph function from transit time measurements
Ogasawara et al[101]	37	25 mg in 5 ml	Subdermal subareolar (3 ml); subdermal peritumour (2 ml)	PDE	Evaluation of the number of lymphatic pathways in patients with breast cancer
Sevick-Muraca et al[1]	24	0.31–100 μg in 0.1–0.3 and 1–3 ml	Intradermal subcutaneous	FDPM imager	Determination of the minimum microdose of ICG for transcutaneous lymph tracking to sentinel lymph nodes in patients with breast cancer and showed active lymph propulsion
Suzuki et al[102]	54	1.5–3 mg in 0.3 ml	Subcutaneously in dorsum of foot	PDE	Assessed lymphatic recovery after vein stripping
Kamiya et al[103]	1	7.5 mg in 1.5 ml	Subcutaneous in bilateral inguinal region	PDE	Located lymphatic fistula causing thorax following oesophagectomy
Rasmussen et al[22]	44	0.4 mg in 1.6 ml	Intradermal	FDPM imager	Assessment of lymphatic architecture and propulsive transport in arms and legs
Unno et al[104]	65	3 mg in 0.6 ml	Subcutaneous injection in dorsum of foot	PDE	Measured lymphatic pressure with inflatable cuff
Adams et al[105]	9	0.3 mg in 1.2 ml	Intradermal injection	FDPM imager	Assessed movement of ICG before and after pneumatic compression therapy in arms
Tan et al[106]	20	0.4 mg in 1.6 ml	Intradermal	FDPM imager	Assessment of lymphatic contractile function after manual lymphatic drainage in arms and legs
Furukawa et al[107]	9	(Not specified) in 0.2 ml	Intracutaneously into the dorsal aspect of each second web space	PDE	Targeting dermal lymphatic backflow during microsurgical lymphaticovenous implantation
Mukenge et al[108]	11	(Not specified) in 0.2–1.0 ml	Subcutaneous	PDE	Assessment of the patency of LVA after surgery
Mihara et al[17]	6	(Not specified) in 0.2 ml	Intracutaneously into the dorsal aspect of the foot (first web space)	PDE	Identifying subcutaneous lymph vessels before and during scarless LVA
Yamamoto et al[109]	20	0.5 mg in 0.2 ml	Subcutaneous in arms and the second web space of the hand	PDE	Proposed classification system for arm lymphoedema

(Continued)

Table 5. (Continued)

Study	Number of subjects	Total dose of ICG	Injection site	Device	Comments
Yamamoto et al[110]	45	1 mg in 0.4 ml	Subcutaneous in leg and first web space of the foot	PDE	Proposed classification system for leg lymphoedema
Yamamoto et al[111]	62	0.5 mg in 0.2 ml	Subcutaneous in leg and first web space of the foot	PDE	Assessed ICG imaging as a means to diagnose subclinical lymphoedema
Unno et al[112]	399	3 mg in 0.6 ml	Subcutaneous	PDE	Assessed the effect of age and gender on lymphatic function
Yamamoto et al[113]	5	0.04 mg in 0.3 ml	Subcutaneous	PDE	Imaging of lymphatics in normal controls and patients with head and neck lymphoedema
Aldrich et al[114]	24	0.3 mg in 1.2 ml	Intradermal	FDPM imager	Assessed systemic progression of lymphoedema in breast cancer survivors
Maus et al[115]	1	0.225 mg in 0.9 ml	Intradermal	FDPM imager	Imaging of lymphatics in head and neck lymphoedema used to redirect manual lymphatic drainage
Akita et al[116]	134	(Not specified) in 0.6 ml	Web spaces of feet	PDE	Showed that ICG lymphography could detect earlier stages of lymphoedema than does lymphoscintigraphy
Akita et al[122]	100	(Not specified) in 0.6 ml	Subcutaneously at the first web space of the foot	PDE	Determination of early stage lymphoedema after lymph node dissection in gynaecological cancer based on the detected patterns
Sakurai et al[117]	327	(Not specified) in 0.15 ml	Subcutaneously into the interdigital area	PDE	Identifying the risk group of post-operative lymphoedema through axillary reverse mapping
Burrows et al[118]	1	0.3 mg in 1.2 ml	Intradermal	FDPM imager	Imaging of lymphatic abnormalities associated with *RASA1* gene mutations
Liu et al[15]	20	2–4 mg in 0.2–0.4 ml	Subdermal	Leica FL800	Guiding the skin incision site of LVA and assessment of the patency of the anastomosis
Mihara et al[119]	72	2 mg in 0.4 ml	Subcutaneously	PDE	Diagnosed and classified lymphoedema
Shibasaki et al[120]	10	0.25 mg in 0.1 ml (single dose of multiple injections)	Subcutaneously on hands and feet	PDE	Evaluation of the severity of lymphatic dysfunction in infants and neonates with congenital lymphatic pleural effusion and ascites
Tan et al[121]	1	0.050 mg in 0.2 ml	Intradermally on hands and feet	FDPM imager	Imaging of abnormal lymphatic drainage in an infant with post-operative chylothorax to guide surgical management

LVA, lymphovenous anastomoses; PDE, photodynamic eye; RASA1, gene encoding RAS p21 protein activator (GTPase activating protein).
The devices mentioned in the table and their manufacturer details in parenthesis are as follows: Leica FL800 (Leica Microsystems Inc., Buffalo Grove, IL), FDPM imager (University of Texas Health Science Center at Houston, TX), PDE (Hamamatsu Photonics Co., Hamamatsu, Japan).

Figure 4. (a) Static near-infrared fluorescence (NIRF) imaging of indocyanine green (ICG)-laden lymphatics in the arm of a normal subject. Supplementary Video A shows increased lymphatic contractile transport in response to manual lymphatic drainage applied by a trained therapist. (b) Static NIRF imaging of ICG-laden lymphatics in the arm of a breast cancer survivor with lymphoedema in the right extremity as depicted in (c). Supplementary Video B shows the comparative lack of lymphatic propulsion compared with that shown in the arm of a normal subject shown in (a). Reproduced from Tan et al,[106] with permission from Elsevier.

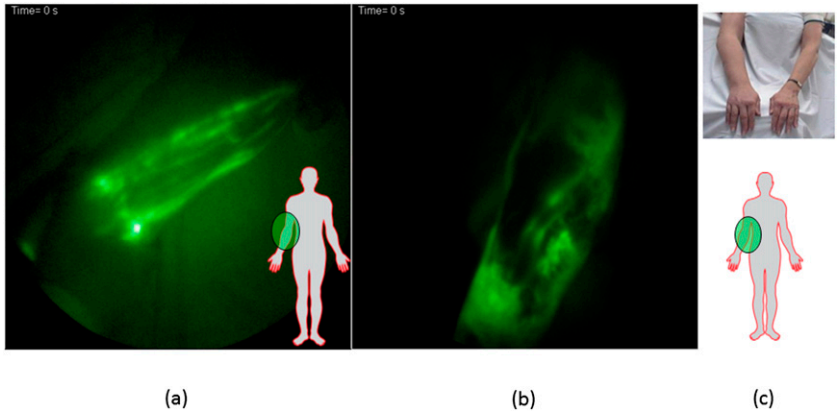

normal lymphatic vasculature in Figure 4a (Supplementary Video A), impaired transit time measurements (*i.e.*, the time between ICG injection and its appearance in the nearest draining lymph nodes) using the PDE device; as well as measurements of reflux or impaired lymphatic propulsion using the FDPM device (Figure 4b; Supplementary Video B). Using the PDE device, Mihara et al[20] showed NIRF imaging to be a superior diagnostic to lymphoscintigraphy when evaluating for lymphoedema. NIRF imaging has also been used to detect lymphatic abnormalities before the onset of swelling symptoms using the FDPM imager,[21,22] earlier than lymphoscintigraphy[122] and following cancer surgery.[68] Using both devices, multiple intradermal injections of single ICG doses were used for lymphatic mapping, typically 0.025 mg in 0.1 ml saline using the FDPM imager and 0.5 mg in 0.1 ml water using the PDE device. Assessment of lymphatic architecture and transport was also performed with NIRF imaging devices in subjects with head and neck lymphoedema[113,115] and used in the treatment setting to assess the effect of lymphoedema treatments, *i.e.* manual lymphatic drainage and pneumatic compression devices, on lymphatic function.[105,106,115] The results suggest the ability to use NIRF imaging to direct therapy and to stratify which subjects could benefit by these non-surgical therapies on the basis of stimulated lymphatic pumping or lymphatic vessel recruitment. LVA, a surgical therapy for late-stage and severe lymphoedema, also uses NIRF imaging in a therapeutic setting to stratify patients who would benefit from the treatment,[122] to guide the skin incision site,[15,17] identify functional subcutaneous and dermal lymphatic vessel LVA[16,17,107] and assess patency of LVA after surgery.[15,108] In another application, NIRF imaging has been used to perform axillary reverse mapping in patients with breast cancer, to identify those lymph nodes that are drained by the arm and thus could be potentially spared in lymph node dissection to prevent later the onset of upper extremity lymphoedema.[101,117,123–125] Lymphatic mapping using NIRF imaging has also been used to provide a lymphatic phenotype for genotyping;[118] to evaluate the lymphatics in infants and neonates with lymphatic pleural effusion and ascites;[120] and to direct surgical management of post-operative chylothorax in infants.[121]

PHANTOMS FOR ASSESSING CLINICAL PERFORMANCE

Currently, the success of NIRF imaging is based upon the ability of the device to detect ICG in humans, as outlined in Tables 2–5, with the expectation that "first-in-human" molecularly targeted imaging agents can likewise be detected by these devices already employed to detect ICG. ICG is comparatively dim compared with other emerging NIR fluorophores, such as IRDye800® (Li-Cor Biosciences, Lincoln, NE) and others,[57] which promise brighter fluorescent signals and the ability to detect targeted tissues deeper and with smaller concentrations than is used for haemo- and lymphovascular imaging of ICG. Device performance is critical and depends upon optimal excitation of NIRF imaging agents, rejection of backscattered excitation and ambient light, and selective collection of fluorescence emanating from the fluorophore. While instrument design differs widely (Table 1), and NIRF molecularly targeted imaging agents can be expected to have broad spectral characteristics that make them amendable to different devices, there remains no systematic measurement procedure and test to enable prediction that a given molecular imaging agent can be detected in humans by a given NIRF imaging device. Furthermore, as technologies evolve and as NIRF imaging device components change, there remains no standardized means that could track device improvements over time and establish clinical performance without involving clinical trials that are often costly. There is also no standardized measurement and approach to qualify the consistent, equivalent operational status of a single device as a function of clinical usage time. Hence, there is an urgent need to develop working standards that are stable over time and enable qualification of imaging device performance and that decouple the device and drug regulatory processes. For example, if a "first-in-humans"

Table 6. Summary of near-infrared and far-red fluorescent solid phantoms

Phantom	Base material	Scatter	Absorber	Fluorescent dye	Excitation peak (nm)	Emission peak (nm)	Fluorescence stability	Comments
Boehm et al[126]	Gelatin	Milk powder	None	NIR96010	755	790	NS	To determine the concentration-dependent contrast resolution of NIR mammography
Grand et al[127]	Gelatin	Intralipid	Haemoglobin	ICG; Pam78	NS	NS	Long-term stability for both ICG and Pam78 at some wavelengths for a period of 4 weeks (measured weekly)	Assessing NIRF imaging system and training surgeon
Baeten et al[128]	Silicone	White silicone pigments	Black silicone pigments	IR-676 iodide; IR-780 iodide	676; 780	700; 799	Long-term stability during (measured every 2 h) and after the curing process (measured periodically) for IR-676 iodide and IR-780 after curing (approximately 2 months)	The hydrophobic fluorophores (IR-676 and IR-780) embedded within silicone are suitable for diffuse fluorescence tomography standards
	Polyester resin	TiO_2	India ink	Cy5.5; AF 750	675; 749	694; 775	Unstable in the first 24 h (measured every 2 h) and then fairly steady degradation after curing (measured periodically) for Cy5.5 over a period of 2 months; unstable during the curing process for AF 750 dye	
Pleijhuis et al[129]	Gelatin	Intralipid	Haemoglobin	ICG	780	820	NS	Assessing intraoperative techniques
Zhu et al[27]	Polyurethane	None	None	QDots 800	None	800	Long-term stability over a 3-month period after curing (measured periodically)	High reflectance to quantify excitation light leakage
Zhu et al[25]	Polyurethane	TiO_2	None	QDots 800	None	800	Long-term stability over a 3-month period after curing (measured periodically)	Different concentrations of QDots 800 to assess the performance of NIRF imaging systems
XFM-2 Fluorescent Phantom	Polyurethane	NS	None	AF 680; AF750; QDots 800	640; 745; none	700; 800; 800	Up to 60% reduction in fluorescent activity over a 4-month period	To test fluorescent imaging, spectral unmixing or fluorescent tomography

AF 680, Alexa Fluor 680 (Invitrogen, Carlsbad, CA); AF 750, Alexa Fluor 750 (Invitrogen); Cy5.5, cyanine dye 5.5 (Amershan Biosciences, Piscataway, NJ); Gelatin (Sofertgelatine; RUF Lebensmittelwork, Quakenbrück, Germany; ICG, indocyanine green; NIRF, near-infrared fluorescence; NS, not specified; QDots 800, Quantum Dots 800 (Qdot® 800 ITk™, Q21 771MP, Invitrogen); TiO_2, titania or titanium dioxide.
IR-676 and IR-780 iodide (Sigma-Aldrich Chemical Company, Inc., Milwaukee, WI), NIR96010 (Institut for Diagnostikforshuing, Schering AG, Berlin, Germany) XFM-2 Fluorescent Phantom (Caliper Life Science, Hopkinton, MA).

imaging agent fails to demark a diseased tissue, how is one to determine whether it was the imaging agent that failed to target the diseased tissue or whether the imaging device was not sensitive enough for its detection? The ICG dose escalation studies by Sevick-Muraca et al[1] and Mieog et al[41] provide important information for setting the dosing and detection levels of imaging agents to begin safety and toxicity studies for eventual translation but inevitably are specific to the particular imaging device used.

Many groups have embarked on the process to construct solid phantoms for quantifying the performance of complete NIRF imaging systems, as well as for comparing systems.[25] While past work has focused upon adding fluorophore or imaging agent in milk or intralipid solutions, these liquid standards have a finite shelf life, are not often replicable and require comprehensive characterization for each use. Table 6 summarizes the developmental efforts found in the literature that seek to establish solid phantoms in which a fluorophore or luminescent material is embedded in a solid medium that mimics or exaggerates tissue-scattering properties.[25,27,126–129] These phantoms are essential to sensitively and accurately detect changes in device performance during manufacture, installation and operation in the clinic. Because ambient light can change with time in the environment, the use of the standards at the point of care can define the expected performance of the device. Hence, if the ICG is not detected during lymphatic mapping in a specific site, then one can safety assume that there are no functional lymphatics to be visualized. Likewise, if a molecular imaging agent is not detected, one can conclude that the molecular imaging agent was not present in or subsurface to the FOV. Long-term stability (>1 year) of these phantoms remains elusive, and while promising candidates are under development, as shown in Table 6, there needs to be an adoption of an industry standard to promote further technological evolution of NIRF devices and their use with emerging NIRF imaging agents.

SUMMARY

NIRF imaging is rapidly emerging for clinical characterization of the lymphatic vasculature, whether for SLN mapping in cancer surgeries or for assessing lymphatic vessel architecture and function in health and a variety of diseases. Herein, we summarized the performance variety of NIRF imaging devices used in the clinic to detect ICG, the only NIR excitable dye currently used in humans. The performance of these devices, while variable, offers promise for the emerging NIRF molecular imaging agents that promise profound impact in surgical and non-surgical applications. Now that there is a plethora of NIRF devices in the clinic and a range of ICG doses used as summarized herein, a critical evaluation of the efficient approaches to evolve to the next step of using "first-in-humans," molecularly targeted imaging agents is needed.

FUNDING

The work was compiled under grant support National Institutes of Health U54 CA136404 and R01 HL09232 (EMS).

ACKNOWLEDGMENTS

We thank Dr John C Rasmussen for reviewing the contribution.

REFERENCES

1. Sevick-Muraca EM, Sharma R, Rasmussen JC, Marshall MV, Wendt JA, Pham HQ, et al. Imaging of lymph flow in breast cancer patients after microdose administration of a near-infrared fluorophore: feasibility study. *Radiology* 2008; **246**: 734–41. doi: 10.1148/radiol.2463070962
2. Unno N, Nishiyama M, Suzuki M, Yamamoto N, Inuzuka K, Sagara D, et al. Quantitative lymph imaging for assessment of lymph function using indocyanine green fluorescence lymphography. *Eur J Vasc Endovascular Surg* 2008; **36**: 230–6. doi: 10.1016/j.ejvs.2008.04.013
3. Darne C, Lu Y, Sevick-Muraca EM. Small animal fluorescence and bioluminescence tomography: a review of approaches, algorithms and technology update. *Phys Med Biol* 2014; **59**: R1–64. doi: 10.1088/0031-9155/59/1/R1
4. Leblond F, Davis SC, Valdés PA, Pogue BW. Pre-clinical whole-body fluorescence imaging: Review of instruments, methods and applications. *J Photochem Photobiol B: Biol* 2010; **98**: 77–94. doi: 10.1016/j.jphotobiol.2009.11.007
5. Weissleder R, Ntziachristos V. Shedding light onto live molecular targets. *Nat Med* 2003; **9**: 123–8.
6. Gurfinkel M, Ke S, Wen X, Li C, Sevick-Muraca EM. Near-infrared fluorescence optical imaging and tomography. *Dis Markers* 2004; **19**: 107–21.
7. Contag CH, Fraser S, Weissleder R. Strategies in *in vivo* molecular imaging. *NeoReviews* 2000; **1**: e225–32.
8. Alander JT, Kaartinen I, Laakso A, Pätilä T, Spillmann T, Tuchin VV, et al. A review of indocyanine green fluorescent imaging in surgery. *Int J Biomed Imaging* 2012; **2012**: 94085. doi: 10.1155/2012/940585
9. Giraudeau C, Moussaron A, Stallivieri A, Mordon S, Frochot C. Indocyanine green: photosensitizer or chromophore? Still a debate. *Curr Med Chem* 2014; **21**: 1871–97.
10. Schaafsma BE, Mieog JSD, Hutteman M, Van der Vorst JR, Kuppen PJK, Löwik CW, et al. The clinical use of indocyanine green as a near-infrared fluorescent contrast agent for image-guided oncologic surgery. *J Surg Oncol* 2011; **104**: 323–32. doi: 10.1002/jso.21943
11. Sevick-Muraca EM, Lopez G, Reynolds JS, Troy TL, Hutchinson CL. Fluorescence and absorption contrast mechanisms for biomedical optical imaging using frequency-domain techniques. *Photochem Photobiol* 1997; **66**: 55–64.
12. Kaiser M, Yafi A, Cinat M, Choi B, Durkin AJ. Noninvasive assessment of burn wound severity using optical technology: a review of current and future modalities. *Burns* 2011; **37**: 377–86. doi: 10.1016/j.burns.2010.11.012
13. Polom K, Murawa D, Rho YS, Nowaczyk P, Hünerbein M, Murawa P. Current trends and emerging future of indocyanine green usage in surgery and oncology. *Cancer* 2011; **117**: 4812–22. doi: 10.1002/cncr.26087
14. Marshall MV, Rasmussen JC, Tan IC, Aldrich MB, Adams KE, Wang X, et al.

Near-infrared fluorescence imaging in humans with indocyanine green: a review and update. *Open Surg Oncol J* 2010; **2**: 12–25.
15. Liu HL, Pang SY, Chan YW. The use of a microscope with near-infrared imaging function in indocyanine green lymphography and lymphaticovenous anastomosis. *J Plast Reconstr Aesthet Surg* 2014; **67**: 231–6. doi: 10.1016/j.bjps.2013.10.039
16. Ogata F, Narushima M, Mihara M, Azuma R, Morimoto Y, Koshima I. Intraoperative lymphography using indocyanine green dye for near-infrared fluorescence labeling in lymphedema. *Ann Plast Surg* 2007; **59**: 180–4.
17. Mihara M, Hara H, Kikuchi K, Yamamoto T, Iida T, Narushima M, et al. Scarless lymphatic venous anastomosis for latent and early-stage lymphoedema using indocyanine green lymphography and non-invasive instruments for visualising subcutaneous vein. *J Plast Reconstr Aesthet Surg* 2012; **65**: 1551–8. doi: 10.1016/j.bjps.2012.05.026
18. Sevick-Muraca EM, Kwon S, Rasmussen JC. Emerging lymphatic imaging technologies for mouse and man. *J Clin Invest* 2014; **124**: 905–14. doi: 10.1172/JCI71612
19. Sevick-Muraca EM. Translation of near-infrared fluorescence imaging technologies: emerging clinical applications. *Annu Rev Med* 2012; **63**: 217–31. doi: 10.1146/annurev-med-070910-083323
20. Mihara M, Hara H, Araki J, Kikuchi K, Narushima M, Yamamoto T, et al. Indocyanine green (ICG) lymphography is superior to lymphoscintigraphy for diagnostic imaging of early lymphedema of the upper limbs. *PLoS One* 2012; **7**: e38182. doi: 10.1371/journal.pone.0038182
21. Rasmussen JC, Tan IC, Marshall MV, Fife CE, Sevick-Muraca EM. Lymphatic imaging in humans with near-infrared fluorescence. *Curr Opin Biotechnol* 2009; **20**: 74–82. doi: 10.1016/j.copbio.2009.01.009
22. Rasmussen JC, Tan IC, Marshall MV, Adams KE, Kwon S, Fife CE, et al. Human lymphatic architecture and dynamic transport imaged using near-infrared fluorescence. *Transl Oncol* 2010; **3**: 362–72.
23. Vahrmeijer AL, Hutteman M, van der Vorst JR, van de Velde CJH, Frangioni JV. Image-guided cancer surgery using near-infrared fluorescence. *Nat Rev Clin Oncol* 2013; **10**: 507–18. doi: 10.1038/nrclinonc.2013
24. Sevick-Muraca EM, Rasmussen JC. Molecular imaging with optics: primer and case for near-infrared fluorescence techniques in personalized medicine. *J Biomed Opt* 2008; **13**: 041303. doi: 10.1117/1.2953185
25. Zhu B, Rasmussen JC, Sevick-Muraca EM. A matter of collection and detection for intraoperative and noninvasive near-infrared fluorescence molecular imaging: to see or not to see? *Med Phys* 2014; **41**: 022105. doi: 10.1118/1.4862514
26. Zhu B, Rasmussen JC, Lu Y, Sevick-Muraca EM. Reduction of excitation light leakage to improve near-infrared fluorescence imaging for tissue surface and deep tissue imaging. *Med Phys* 2010; **37**: 5961–70.
27. Zhu B, Tan IC, Rasmussen JC, Sevick-Muraca EM. Validating the sensitivity and performance of near-infrared fluorescence imaging and tomography devices using a novel solid phantom and measurement approach. *Technol Cancer Res Treat* 2012; **11**: 95–104.
28. Anzai Y, Blackwell KE, Hirschowitz SL, Rogers JW, Sato Y, Yuh WT, et al. Initial clinical experience with dextran-coated superparamagnetic iron oxide for detection of lymph node metastases in patients with head and neck cancer. *Radiology* 1994; **192**: 709–15.
29. Wallace AM, Han LK, Povoski SP, Deck K, Schneebaum S, Hall NC, et al. Comparative evaluation of [(99m)tc] tilmanocept for sentinel lymph node mapping in breast cancer patients: results of two phase 3 trials. *Ann Surg Oncol* 2013; **20**: 2590–9. doi: 10.1245/s10434-013-2887-8
30. Hall MA, Pinkston KL, Wilganowski N, Robinson H, Ghosh P, Azhdarinia A, et al. Comparison of mAbs targeting epithelial cell adhesion molecule for the detection of prostate cancer lymph node metastases with multimodal contrast agents: quantitative small-animal PET/CT and NIRF. *J Nucl Med* 2012; **53**: 1427–37. doi: 10.2967/jnumed.112.106302
31. Heath CH, Deep NL, Sweeny L, Zinn KR, Rosenthal EL. Use of panitumumab-IRDye800 to image microscopic head and neck cancer in an orthotopic surgical model. *Ann Surg Oncol* 2012; **19**: 3879–87. doi: 10.1245/s10434-012-2435-y
32. Gao P, Pinkston KL, Wilganowski N, Robinson H, Zhu B, Sevick-Muraca EM, et al. Deglycosylation of mAb by EndoS for improved molecular imaging sensitivity. *Mol Imaging Biol*; in press. Epub ahead of print August 2014. doi: 10.1007/s11307-014-0781-9
33. Kitai T, Inomoto T, Miwa M, Shikayama T. Fluorescence navigation with indocyanine green for detecting sentinel lymph nodes in breast cancer. *Breast Cancer* 2005; **12**: 211–15.
34. Tagaya N, Yamazaki R, Nakagawa A, Abe A, Hamada K, Kubota K, et al. Intraoperative identification of sentinel lymph nodes by near-infrared fluorescence imaging in patients with breast cancer. *Am J Surg* 2008; **195**: 850–3. doi: 10.1016/j.amjsurg.2007.02.032
35. Murawa D, Hirche C, Dresel S, Hünerbein M. Sentinel lymph node biopsy in breast cancer guided by indocyanine green fluorescence. *Br J Surg* 2009; **96**: 1289–94. doi: 10.1002/bjs.6721
36. Troyan SL, Kianzad V, Gibbs-Strauss SL, Gioux S, Matsui A, Oketokoun R, et al. The FLARE intraoperative near-infrared fluorescence imaging system: a first-in-human clinical trial in breast cancer sentinel lymph node mapping. *Ann Surg Oncol* 2009; **16**: 2943–52. doi: 10.1245/s10434-009-0594-2
37. Sugie T, Kassim KA, Takeuchi M, Hashimoto T, Yamagami K, Masai Y, et al. A novel method for sentinel lymph node biopsy by indocyanine green fluorescence technique in breast cancer. *Cancers* 2010; **2**: 713–20. doi: 10.3390/cancers2020713
38. Hirche C, Murawa D, Mohr Z, Kneif S, Hünerbein M. ICG fluorescence-guided sentinel node biopsy for axillary nodal staging in breast cancer. *Breast Cancer Res Treat* 2010; **121**: 373–8. doi: 10.1007/s10549-010-0760-z
39. Hojo T, Nagao T, Kikuyama M, Akashi S, Kinoshita T. Evaluation of sentinel node biopsy by combined fluorescent and dye method and lymph flow for breast cancer. *Breast* 2010; **19**: 210–13. doi: 10.1016/j.breast.2010.01.014
40. Tagaya N, Aoyagi H, Nakagawa A, Abe A, Iwasaki Y, Tachibana M, et al. A novel approach for sentinel lymph node identification using fluorescence imaging and image overlay navigation surgery in patients with breast cancer. *World J Surg* 2011; **35**: 154–8. doi: 10.1007/s00268-010-0811-y
41. Mieog JSD, Troyan SL, Hutteman M, Donohoe KJ, van der Vorst JR, Stockdale A, et al. Toward optimization of imaging system and lymphatic tracer for near-infrared fluorescent sentinel lymph node mapping in breast cancer. *Ann Surg Oncol* 2011; **18**: 2483–91. doi: 10.1245/s10434-011-1566-x
42. Hutteman M, Mieog JS, van der Vorst JR, Liefers GJ, Putter H, Löwik CW, et al. Randomized, double-blind comparison of indocyanine green with or without albumin premixing for near-infrared fluorescence imaging of sentinel lymph nodes in breast cancer patients. *Breast Cancer Res Treat* 2011; **127**: 163–70. doi: 10.1007/s10549-011-1419-0
43. Abe H, Mori T, Umeda T, Tanaka M, Kawai Y, Shimizu T, et al. Indocyanine green fluorescence imaging system for

sentinel lymph node biopsies in early breast cancer patients. *Surg Today* 2011; **41**: 197–202.
44. Aoyama K, Kamio T, Ohchi T, Nishizawa M, Kameoka S. Sentinel lymph node biopsy for breast cancer patients using fluorescence navigation with indocyanine green. *World J Surg Oncol* 2011; **9**: 157. doi: 10.1186/1477-7819-9-157
45. van der Vorst JR, Schaafsma BE, Verbeek FP, Hutteman M, Mieog JS, Lowik CW, et al. Randomized comparison of near-infrared fluorescence imaging using indocyanine green and 99m technetium with or without patent blue for the sentinel lymph node procedure in breast cancer patients. *Ann Surg Oncol* 2012; **19**: 4104–11. doi: 10.1245/s10434-012-2466-4
46. Wishart GC, Loh SW, Jones L, Benson JR. A feasibility study (ICG-10) of indocyanine green (ICG) fluorescence mapping for sentinel lymph node detection in early breast cancer. *Eur J Surg Oncol* 2012; **38**: 651–6. doi: 10.1016/j.ejso.2012.05.007
47. Hirano A, Kamimura M, Ogura K, Kim N, Hattori A, Setoguchi Y, et al. A comparison of indocyanine green fluorescence imaging plus blue dye and blue dye alone for sentinel node navigation surgery in breast cancer patients. *Ann Surg Oncol* 2012; **19**: 4112–16. doi: 10.1245/s10434-012-2478-0
48. Takeuchi M, Sugie T, Abdelazeem K, Kato H, Shinkura N, Takada M, et al. Lymphatic mapping with fluorescence navigation using indocyanine green and axillary surgery in patients with primary breast cancer. *Breast J* 2012; **18**: 535–41. doi: 10.1111/tbj.12004
49. Polom K, Murawa D, Nowaczyk P, Rho YS, Murawa P. Breast cancer sentinel lymph node mapping using near infrared guided indocyanine green and indocyanine green–human serum albumin in comparison with gamma emitting radioactive colloid tracer. *Eur J Surg Oncol* 2012; **38**: 137–42. doi: 10.1016/j.ejso.2011.11.004
50. Sugie T, Sawada T, Tagaya N, Kinoshita T, Yamagami K, Suwa H, et al. Comparison of the indocyanine green fluorescence and blue dye methods in detection of sentinel lymph nodes in early-stage breast cancer. *Ann Surg Oncol* 2013; **20**: 2213–18. doi: 10.1245/s10434-013-2890-0
51. Schaafsma BE, Verbeek FP, Rietbergen DD, van der Hiel B, van der Vorst JR, Liefers GJ, et al. Clinical trial of combined radio-and fluorescence-guided sentinel lymph node biopsy in breast cancer. *Br J Surg* 2013; **100**: 1037–44. doi: 10.1002/bjs.9159
52. Jung SY, Kim SK, Kim SW, Kwon Y, Lee ES, Kang HS, et al. Comparison of sentinel lymph node biopsy guided by the multimodal method of indocyanine green fluorescence, radioisotope, and blue dye versus the radioisotope method in breast cancer: a randomized controlled trial. *Ann Surg Oncol* 2013; **21**: 1254–9. doi: 10.1245/s10434-013-3437-0
53. Guo W, Zhang L, Ji J, Gao W, Liu J, Tong M. Breast cancer sentinel lymph node mapping using near-infrared guided indocyanine green in comparison with blue dye. *Tumor Biol* 2014; **35**: 3073–8. doi: 10.1007/s13277-013-1399-2
54. Chi C, Ye J, Ding H, He D, Huang W, Zhang G-J, et al. Use of indocyanine green for detecting the sentinel lymph node in breast cancer patients: from preclinical evaluation to clinical validation. *PLoS One* 2013; **8**: e83927. doi: 10.1371/journal.pone.0083927
55. Ballardini B, Santoro L, Sangalli C, Gentilini O, Renne G, Lissidini G, et al. The indocyanine green method is equivalent to the ^{99m}Tc-labeled radiotracer method for identifying the sentinel node in breast cancer: a concordance and validation study. *Eur J Surg Oncol* 2013; **39**: 1332–6. doi: 10.1016/j.ejso.2013.10.004
56. Verbeek FP, Troyan SL, Mieog JS, Liefers GJ, Moffitt LA, Rosenberg M, et al. Near-infrared fluorescence sentinel lymph node mapping in breast cancer: a multicenter experience. *Breast Cancer Res Treat* 2014; **143**: 333–42. doi: 10.1007/s10549-013-2802-9
57. Azhdarinia A, Ghosh P, Ghosh S, Wilganowski N, Sevick-Muraca EM. Dual-labeling strategies for nuclear and fluorescence molecular imaging: a review and analysis. *Mol Imaging Biol* 2011; **14**: 261–76. doi: 10.1007/s11307-011-0528-9
58. Fujiwara M, Mizukami T, Suzuki A, Fukamizu H. Sentinel lymph node detection in skin cancer patients using real-time fluorescence navigation with indocyanine green: preliminary experience. *J Plast Reconstr Aesthet Surg* 2009; **62**: e373–8. doi: 10.1016/j.bjps.2007.12.074
59. Tsujino Y, Mizumoto K, Matsuzaka Y, Niihara H, Morita E. Fluorescence navigation with indocyanine green for detecting sentinel nodes in extramammary Paget's disease and squamous cell carcinoma. *J Dermatol* 2009; **36**: 90–4. doi: 10.1111/j.1346-8138.2009.00595.x
60. Tanaka R, Nakashima K, Fujimoto W. Sentinel lymph node detection in skin cancer using fluorescence navigation with indocyanine green. *J Dermatol* 2009; **36**: 468–70. doi: 10.1111/j.1346-8138.2009.00679.x
61. Mizukami T, Fujiwara M, Suzuki A, Nagata T, Fukamizu H. Sentinel lymph node detection by indocyanine green fluorescence imaging in skin cancer patients: technical refinement. *Open Surg Oncol J* 2010; **2**: 57–61.
62. Namikawa K, Yamazaki N. Sentinel lymph node biopsy guided by indocyanine green fluorescence for cutaneous melanoma. *Eur J Dermatol* 2011; **21**: 184–90. doi: 10.1684/ejd.2010.1237
63. Fujisawa Y, Nakamura Y, Kawachi Y, Otsuka F. A custom-made, low-cost intraoperative fluorescence navigation system with indocyanine green for sentinel lymph node biopsy in skin cancer. *Dermatology* 2011; **222**: 261–8. doi: 10.1159/000327080
64. Hayashi T, Furukawa H, Oyama A, Funayama E, Saito A, Yamao T, et al. Sentinel lymph node biopsy using real-time fluorescence navigation with indocyanine green in cutaneous head and neck/lip mucosa melanomas. *Head Neck* 2012; **34**: 758–61. doi: 10.1002/hed.21651
65. Stoffels I, von der Stück H, Boy C, Pöppel T, Körber N, Weindorf M, et al. Indocyanine green fluorescence-guided sentinel lymph node biopsy in dermato-oncology. *J Dtsch Dermatol Ges* 2012; **10**: 51–7. doi: 10.1111/j.1610-0387.2011.07843.x
66. Polom K, Murawa D, Rho YS, Spychala A, Murawa P. Skin melanoma sentinel lymph node biopsy using real-time fluorescence navigation with indocyanine green and indocyanine green with human serum albumin. *Br J Dermatol* 2012; **166**: 682–3. doi: 10.1111/j.1365-2133.2011.10634.x
67. Fujisawa Y, Nakamura Y, Kawachi Y, Otsuka F. Indocyanine green fluorescence-navigated sentinel node biopsy showed higher sensitivity than the radioisotope or blue dye method, which may help to reduce false-negative cases in skin cancer. *J Surg Oncol* 2012; **106**: 41–5. doi: 10.1002/jso.23045
68. Rasmussen JC, Kwon S, Sevick-Muraca EM, Cormier JN. The role of lymphatics in cancer as assessed by near-infrared fluorescence imaging. *Ann Biomed Eng* 2012; **40**: 408–21. doi: 10.1007/s10439-011-0476-1
69. van der Vorst JR, Schaafsma BE, Verbeek FP, Swijnenburg RJ, Hutteman M, Liefers GJ, et al. Dose optimization for near-infrared fluorescence sentinel lymph node mapping in patients with melanoma. *Br J Dermatol* 2013; **168**: 93–8. doi: 10.1111/bjd.12059
70. Namikawa K, Tsutsumida A, Tanaka R, Kato J, Yamazaki N. Limitation of indocyanine green fluorescence in identifying sentinel lymph node prior to skin incision in cutaneous melanoma. *Int J Clin Oncol* 2013; **19**: 198–203. doi: 10.1007/s10147-013-0524-y

71. Gilmore DM, Khullar OV, Gioux S, Stockdale A, Frangioni JV, Colson YL, et al. Effective low-dose escalation of indocyanine green for near-infrared fluorescent sentinel lymph node mapping in melanoma. *Ann Surg Oncol* 2013; **20**: 2357–63. doi: 10.1245/s10434-013-2905-x
72. Nakamura Y, Fujisawa Y, Nakamura Y, Maruyama H, Furuta J-i, Kawachi Y, et al. Improvement of the sentinel lymph node detection rate of cervical sentinel lymph node biopsy using real-time fluorescence navigation with indocyanine green in head and neck skin cancer. *J Dermatol* 2013; **40**: 453–7. doi: 10.1111/1346-8138.12158
73. Miyashiro I, Miyoshi N, Hiratsuka M, Kishi K, Yamada T, Ohue M, et al. Detection of sentinel node in gastric cancer surgery by indocyanine green fluorescence imaging: comparison with infrared imaging. *Ann Surg Oncol* 2008; **15**: 1640–3. doi: 10.1245/s10434-008-9872-7
74. Tajima Y, Yamazaki K, Masuda Y, Kato M, Yasuda D, Aoki T, et al. Sentinel node mapping guided by indocyanine green fluorescence imaging in gastric cancer. *Ann Surg* 2009; **249**: 58–62. doi: 10.1097/SLA.0b013e3181927267
75. Tajima Y, Murakami M, Yamazaki K, Masuda Y, Kato M, Sato A, et al. Sentinel node mapping guided by indocyanine green fluorescence imaging during laparoscopic surgery in gastric cancer. *Ann Surg Oncol* 2010; **17**: 1787–93. doi: 10.1245/s10434-010-0944-0
76. Miyashiro I, Kishi K, Yano M, Tanaka K, Motoori M, Ohue M, et al. Laparoscopic detection of sentinel node in gastric cancer surgery by indocyanine green fluorescence imaging. *Surg Endosc* 2011; **25**: 1672–6. doi: 10.1007/s00464-010-1405-3
77. Yoshida M, Kubota K, Kuroda J, Ohta K, Nakamura T, Saito J, et al. Indocyanine green injection for detecting sentinel nodes using color fluorescence camera in the laparoscopy-assisted gastrectomy. *J Gastroenterol Hepatol* 2012; **27**: 29–33. doi: 10.1111/j.1440-1746.2012.07067.x
78. Watanabe M, Tsunoda A, Narita K, Kusano M, Miwa M. Colonic tattooing using fluorescence imaging with light-emitting diode-activated indocyanine green: a feasibility study. *Surg Today* 2009; **39**: 214–18. doi: 10.1007/s00595-008-3849-9
79. Noura S, Ohue M, Seki Y, Tanaka K, Motoori M, Kishi K, et al. Feasibility of a lateral region sentinel node biopsy of lower rectal cancer guided by indocyanine green using a near-infrared camera system. *Ann Surg Oncol* 2010; **17**: 144–51. doi: 10.1245/s10434-009-0711-2
80. Hirche C, Dresel S, Krempien R, Hünerbein M. Sentinel node biopsy by indocyanine green retention fluorescence detection for inguinal lymph node staging of anal cancer: preliminary experience. *Ann Surg Oncol* 2010; **17**: 2357–62. doi: 10.1245/s10434-010-1010-7
81. Hirche C, Mohr Z, Kneif S, Doniga S, Murawa D, Strik M, et al. Ultrastaging of colon cancer by sentinel node biopsy using fluorescence navigation with indocyanine green. *Int J Colorectal Dis* 2012; **27**: 319–24. doi: 10.1007/s00384-011-1306-5
82. Cahill RA, Anderson M, Wang LM, Lindsey I, Cunningham C, Mortensen NJ. Near-infrared (NIR) laparoscopy for intraoperative lymphatic road-mapping and sentinel node identification during definitive surgical resection of early-stage colorectal neoplasia. *Surg Endosc* 2012; **26**: 197–204. doi: 10.1007/s00464-011-1854-3
83. Manny TB, Hemal AK. Fluorescence-enhanced robotic radical cystectomy using unconjugated indocyanine green for pelvic lymphangiography, tumor marking, and mesenteric angiography: the initial clinical experience. *Urology* 2014; **83**: 824–30. doi: 10.1016/j.urology.2013.11.042
84. Manny TB, Patel M, Hemal AK. Fluorescence-enhanced robotic radical prostatectomy using real-time lymphangiography and tissue marking with percutaneous injection of unconjugated indocyanine green: the initial clinical experience in 50 patients. *Eur Urol* 2014; **65**: 1162–8. doi: 10.1016/j.eururo.2013.11.017
85. Furukawa N, Oi H, Yoshida S, Shigetomi H, Kanayama S, Kobayashi H. The usefulness of photodynamic eye for sentinel lymph node identification in patients with cervical cancer. *Tumori* 2010; **96**: 936–40.
86. Crane LM, Themelis G, Pleijhuis RG, Harlaar NJ, Sarantopoulos A, Arts HJ, et al. Intraoperative multispectral fluorescence imaging for the detection of the sentinel lymph node in cervical cancer: a novel concept. *Mol Imaging Biol* 2011; **13**: 1043–9. doi: 10.1007/s11307-010-0425-7
87. van der Vorst JR, Hutteman M, Gaarenstroom KN, Peters AA, Mieog JS, Schaafsma BE, et al. Optimization of near-infrared fluorescent sentinel lymph node mapping in cervical cancer patients. *Int J Gynecol Cancer* 2011; **21**: 1472. doi: 10.1097/IGC.0b013e31822b451d
88. Rossi EC, Ivanova A, Boggess JF. Robotically assisted fluorescence-guided lymph node mapping with ICG for gynecologic malignancies: a feasibility study. *Gynecol Oncol* 2012; **124**: 78–82. doi: 10.1016/j.ygyno.2011.09.025
89. Schaafsma BE, van der Vorst JR, Gaarenstroom KN, Peters AA, Verbeek FP, de Kroon CD, et al. Randomized comparison of near-infrared fluorescence lymphatic tracers for sentinel lymph node mapping of cervical cancer. *Gynecol Oncol* 2012; **127**: 126–30. doi: 10.1016/j.ygyno.2012.07.002
90. Crane LM, Themelis G, Arts HJ, Buddingh KT, Brouwers AH, Ntziachristos V, et al. Intraoperative near-infrared fluorescence imaging for sentinel lymph node detection in vulvar cancer: first clinical results. *Gynecol Oncol* 2011; **120**: 291–5. doi: 10.1016/j.ygyno.2010.10.009
91. Hutteman M, Van Der Vorst JR, Gaarenstroom KN, Peters AAW, Mieog JSD, Schaafsma BE, et al. Optimization of near-infrared fluorescent sentinel lymph node mapping for vulvar cancer. *Am J Obstetrics Gynecol* 2012; **206**: 89.e1–5. doi: 10.1016/j.ajog.2011.07.039
92. Holloway RW, Bravo RA, Rakowski JA, James JA, Jeppson CN, Ingersoll SB, et al. Detection of sentinel lymph nodes in patients with endometrial cancer undergoing robotic-assisted staging: a comparison of colorimetric and fluorescence imaging. *Gynecol Oncol* 2012; **126**: 25–9. doi: 10.1016/j.ygyno.2012.04.009
93. Rossi EC, Jackson A, Ivanova A, Boggess JF. Detection of sentinel nodes for endometrial cancer with robotic assisted fluorescence imaging: cervical versus hysteroscopic injection. *Int J Gynecol Cancer* 2013; **23**: 1704–11. doi: 10.1097/IGC.0b013e3182a616f6
94. Jewell EL, Huang JJ, Abu-Rustum NR, Gardner GJ, Brown CL, Sonoda Y, et al. Detection of sentinel lymph nodes in minimally invasive surgery using indocyanine green and near-infrared fluorescence imaging for uterine and cervical malignancies. *Gynecol Oncol* 2014; **133**: 274–7. doi: 10.1016/j.ygyno.2014.02.028
95. Bredell MG. Sentinel lymph node mapping by indocyanin green fluorescence imaging in oropharyngeal cancer-preliminary experience. *Head Neck Oncol* 2010; **2**: 31. doi: 10.1186/1758-3284-2-31
96. van den Berg NS, Brouwer OR, Klop WM, Karakullukcu B, Zuur CL, Tan IB, et al. Concomitant radio-and fluorescence-guided sentinel lymph node biopsy in squamous cell carcinoma of the oral cavity using ICG-^{99m}Tc-nanocolloid. *Eur J Nucl Med Mol Imaging* 2012; **39**: 1128–36. doi: 10.1007/s00259-012-2129-5

97. van der Vorst JR, Schaafsma BE, Verbeek FP, Keereweer S, Jansen JC, van der Velden LA, et al. Near-infrared fluorescence sentinel lymph node mapping of the oral cavity in head and neck cancer patients. *Oral Oncol* 2013; **49**: 15–19. doi: 10.1016/j.oraloncology.2012.07.017
98. Yamashita S, Tokuishi K, Anami K, Miyawaki M, Moroga T, Kamei M, et al. Video-assisted thoracoscopic indocyanine green fluorescence imaging system shows sentinel lymph nodes in non-small-cell lung cancer. *J Thorac Cardiovasc Surg* 2011; **141**: 141–4. doi: 10.1016/j.jtcvs.2010.01.028
99. Gilmore DM, Khullar OV, Jaklitsch MT, Chirieac LR, Frangioni JV, Colson YL. Identification of metastatic nodal disease in a phase 1 dose-escalation trial of intraoperative sentinel lymph node mapping in non-small cell lung cancer using near-infrared imaging. *J Thorac Cardiovasc Surg* 2013; **146**: 562–70. doi: 10.1016/j.jtcvs.2013.04.010
100. Unno N, Inuzuka K, Suzuki M, Yamamoto N, Sagara D, Nishiyama M, et al. Preliminary experience with a novel fluorescence lymphography using indocyanine green in patients with secondary lymphedema. *J Vasc Surg* 2007; **45**: 1016–21.
101. Ogasawara Y, Ikeda H, Takahashi M, Kawasaki K, Doihara H. Evaluation of breast lymphatic pathways with indocyanine green fluorescence imaging in patients with breast cancer. *World J Surg* 2008; **32**: 1924–9. doi: 10.1007/s00268-008-9519-7
102. Suzuki M, Unno N, Yamamoto N, Nishiyama M, Sagara D, Tanaka H, et al. Impaired lymphatic function recovered after great saphenous vein stripping in patients with varicose vein: venodynamic and lymphodynamic results. *J Vasc Surg* 2009; **50**: 1085–91. doi: 10.1016/j.jvs.2009.06.003
103. Kamiya K, Unno N, Konno H. Intraoperative indocyanine green fluorescence lymphography, a novel imaging technique to detect a chyle fistula after an esophagectomy: report of a case. *Surg Today* 2009; **39**: 421–4. doi: 10.1007/s00595-008-3852-1
104. Unno N, Nishiyama M, Suzuki M, Tanaka H, Yamamoto N, Sagara D, et al. A novel method of measuring human lymphatic pumping using indocyanine green fluorescence lymphography. *J Vasc Surg* 2010; **52**: 946–52. doi: 10.1016/j.jvs.2010.04.067
105. Adams KE, Rasmussen JC, Darne C, Tan I, Aldrich MB, Marshall MV, et al. Direct evidence of lymphatic function improvement after advanced pneumatic compression device treatment of lymphedema. *Biomed Opt Express* 2010; **1**: 114–25.
106. Tan I, Maus EA, Rasmussen JC, Marshall MV, Adams KE, Fife CE, et al. Assessment of lymphatic contractile function after manual lymphatic drainage using near-infrared fluorescence imaging. *Arch Phys Med Rehabil* 2011; **92**: 756–64.e1. doi: 10.1016/j.apmr.2010.12.027
107. Furukawa H, Osawa M, Saito A, Hayashi T, Funayama E, Oyama A, et al. Microsurgical lymphaticovenous implantation targeting dermal lymphatic backflow using indocyanine green fluorescence lymphography in the treatment of postmastectomy lymphedema. *Plast Reconstr Surg* 2011; **127**: 1804–11. doi: 10.1097/PRS.0b013e31820cf2e2
108. Mukenge SM, Catena M, Negrini D, Ratti F, Moriondo A, Briganti A, et al. Assessment and follow-up of patency after lymphovenous microsurgery for treatment of secondary lymphedema in external male genital organs. *Eur Urol* 2011; **60**: 1114–19. doi: 10.1016/j.eururo.2010.11.020
109. Yamamoto T, Yamamoto N, Doi K, Oshima A, Yoshimatsu H, Todokoro T, et al. Indocyanine green-enhanced lymphography for upper extremity lymphedema: a novel severity staging system using dermal backflow patterns. *Plast Reconstr Surg* 2011; **128**: 941–7. doi: 10.1097/PRS.0b013e3182268cd9
110. Yamamoto T, Narushima M, Doi K, Oshima A, Ogata F, Mihara M, et al. Characteristic indocyanine green lymphography findings in lower extremity lymphedema: the generation of a novel lymphedema severity staging system using dermal backflow patterns. *Plast Reconstr Surg* 2011; **127**: 1979–86. doi: 10.1097/PRS.0b013e31820cf5df
111. Yamamoto T, Matsuda N, Doi K, Oshima A, Yoshimatsu H, Todokoro T, et al. The earliest finding of indocyanine green lymphography in asymptomatic limbs of lower extremity lymphedema patients secondary to cancer treatment: the modified dermal backflow stage and concept of subclinical lymphedema. *Plast Reconstr Surg* 2011; **128**: 314e-21. doi: 10.1097/PRS.0b013e3182268da8
112. Unno N, Tanaka H, Suzuki M, Yamamoto N, Mano Y, Sano M, et al. Influence of age and gender on human lymphatic pumping pressure in the leg. *Lymphology* 2011; **44**: 113–20.
113. Yamamoto T, Lida T, Matsuda N, Kikuchi K, Yoshimatsu H, Mihara M, et al. Indocyanine green (ICG)-enhanced lymphography for evaluation of facial lymphoedema. *J Plast Reconstr Aesthet Surg* 2011; **64**: 1541–4. doi: 10.1016/j.bjps.2011.05.025
114. Aldrich MB, Guilliod R, Fife CE, Maus EA, Smith L, Rasmussen JC, et al. Lymphatic abnormalities in the normal contralateral arms of subjects with breast cancer-related lymphedema as assessed by near-infrared fluorescent imaging. *Biomed Opt Express* 2012; **3**: 1256–65. doi: 10.1364/BOE.3.001256
115. Maus EA, Tan IC, Rasmussen JC, Marshall MV, Fife CE, Smith LA, et al. Near-infrared fluorescence imaging of lymphatics in head and neck lymphedema. *Head Neck* 2012; **34**: 448–53. doi: 10.1002/hed.21538
116. Akita S, Mitsukawa N, Kazama T, Kuriyama M, Kubota Y, Omori N, et al. Comparison of lymphoscintigraphy and indocyanine green lymphography for the diagnosis of extremity lymphoedema. *J Plast Reconstr Aesthet Surg* 2013; **66**: 792–8. doi: 10.1016/j.bjps.2013.02.023
117. Sakurai T, Endo M, Shimizu K, Yoshimizu N, Nakajima K, Nosaka K, et al. Axillary reverse mapping using fluorescence imaging is useful for identifying the risk group of postoperative lymphedema in breast cancer patients undergoing sentinel node biopsies. *J Surg Oncol* 2013; **109**: 612–15. doi: 10.1002/jso.23528
118. Burrows PE, Gonzalez-Garay ML, Rasmussen JC, Aldrich MB, Guilliod R, Maus EA, et al. Lymphatic abnormalities are associated with RASA1 gene mutations in mouse and man. *Proc Natl Acad Sci U S A* 2013; **110**: 8621–6. doi: 10.1073/pnas.1222722110
119. Mihara M, Seki Y, Hara H, Iida T, Oka A, Kikuchi K, et al. Predictive lymphatic mapping: a method for mapping lymphatic channels in patients with advanced unilateral lymphedema using indocyanine green lymphography. *Ann Plast Surg* 2014; **72**: 706–10. doi: 10.1097/SAP.0b013e31826a18b1
120. Shibasaki J, Hara H, Mihara M, Adachi S, Uchida Y, Itani Y. Evaluation of lymphatic dysplasia in patients with congenital pleural effusion and ascites using indocyanine green lymphography. *J Pediatr* 2014; **164**: 1116–20.e1. doi: 10.1016/j.jpeds.2013.12.052
121. Tan IC, Balaguru D, Rasmussen JC, Guilliod R, Bricker JT, Douglas WI, et al. Investigational lymphatic imaging at the bedside in a pediatric postoperative chylothorax patient. *Pediatr Cardiol* 2014; **35**: 1295–300. doi: 10.1007/s00246-014-0946-y

122. Akita S, Mitsukawa N, Rikihisa N, Kubota Y, Omori N, Mitsuhashi A, et al. Early diagnosis and risk factors for lymphedema following lymph node dissection for gynecologic cancer. *Plast Reconstr Surg* 2013; **131**: 283–90. doi: 10.1097/PRS.0b013e318277870f
123. Noguchi M, Noguchi M, Nakano Y, Ohno Y, Kosaka T. Axillary reverse mapping using a fluorescence imaging system in breast cancer. *J Surg Oncol* 2012; **105**: 229–34. doi: 10.1002/jso.22094
124. Ikeda K, Ogawa Y, Komatsu H, Mori Y, Ishikawa A, Nakajima T, et al. Evaluation of the metastatic status of lymph nodes identified using axillary reverse mapping in breast cancer patients. *World J Surg Oncol* 2012; **10**: 233. doi: 10.1186/1477-7819-10-233
125. Meric-Bernstam F, Rasmussen JC, Krishnamurthy S, Tan I, Zhu B, Wagner JL, et al. Toward nodal staging of axillary lymph node basins through intradermal administration of fluorescent imaging agents. *Biomed Opt Express* 2014; **5**: 183–96. doi: 10.1364/BOE.5.000183
126. Boehm T, Hochmuth A, Malich A, Reichenbach JR, Fleck M, Kaiser WA. Contrast-enhanced near-infrared laser mammography with a prototype breast scanner: feasibility study with tissue phantoms and preliminary results of imaging experimental tumors. *Invest Radiol* 2001; **36**: 573–81.
127. Grand AM, Lomnes SJ, Ohnishi S, Morgan TG, Gogbashian A, Frangioni JV, et al. Tissue-like phantoms for near-infrared fluorescence imaging system assessment and the training of surgeons. *J Biomed Opt* 2006; **11**: 014007.
128. Baeten J, Niedre M, Dunham J, Ntziachristos V. Development of fluorescent materials for diffuse fluorescence tomography standards and phantoms. *Opt Express* 2007; **15**: 8681–94.
129. Pleijhuis RG, Langhout GC, Helfrich W, Themelis G, Sarantopoulos A, Crane LM, et al. Near-infrared fluorescence (NIRF) imaging in breast-conserving surgery: assessing intraoperative techniques in tissue-simulating breast phantoms. *Eur J Surg Oncol* 2011; **37**: 32–9. doi: 10.1016/j.ejso.2010.10.006